Journal of Physical and Chemical Studies (JPCS), Volume 1, Issue 4 | April 2026 | pp. 17-56

https://scientia-nexus.org/index.php/jpcs
DOI: https://doi.org/10.5281/zenodo.19767807

An Open-Access Peer-Reviewed Journal

Phyto-Mediated Green Synthesis and Physicochemical Characterization of Titanium Dioxide Nanoparticles for Environmental and Pharmacological Applications

Muhammad Amin[1], Muhammad Amir Abbas[2*], Jamaluddin Mahar[3], Muhammad Shakeel Shahzad[4], Muhammad Shahid Rasool[5]

[1]Department of Chemistry, Superior University, Lahore, Pakistan

[2]Institute of Chemistry, the Islamia University of Bahawalpur, Bahawalpur, Pakistan

[3]Department of Chemistry, Quaid-E-Azam University Islamabad, Islamabad, Pakistan

[4]Institute of Chemistry, Khawaja Fareed University of Engineering and Information Technology Rahim Yar Khan, Pakistan

[5]Departments of Chemistry, University of Karachi, Karachi, Pakistan

Authors E-mails:

1. Muhammad Amin: aminabdulhaq0@gmail.com (M.A)
2. Muhammad Amir Abbas: muhammadamirabbas@gmail.com (M.A.A.)
3. Jamaluddin Mahar: jamaluddin@uosahiwal.edu.pk (J.M.)
4. Muhammad Shakeel Shahzad: shakeel.shahzad3@gmail.com (M.S.S)
5. Muhammad Shahid Rasool: ms.shahidrasool788@gmail.com (M.S.R.)

[*]Corresponding author: E-mail:

Muhammad Amir Abbas: muhammadamirabbas@gmail.com (M.A.A.)

Received: April 5, 2026 Accepted: April 25, 2026

https://scientia-nexus.org/index.php/jpcs
DOI: https://doi.org/10.5281/zenodo.19767807

An Open-Access Peer-Reviewed Journal

Abstract

The development of environmentally sustainable synthesis strategies has become an important focus in nanoscience and nanotechnology. Among these approaches, the green synthesis of metal oxide nanoparticles using plant extracts has attracted significant attention due to its eco-friendly nature, cost-effectiveness, and avoidance of hazardous chemicals associated with conventional physicochemical methods. In the present study, Titanium Dioxide nanoparticles were synthesized through a green route using Acacia nilotica extract as a reducing and stabilizing agent. The biosynthesized nanoparticles were comprehensively characterized using various spectroscopic and microscopic techniques, including UV–Visible spectroscopy (UV–Vis), Dynamic Light Scattering (DLS), Fourier Transform Infrared Spectroscopy (FTIR), X-ray Diffraction (XRD), Scanning Electron Microscopy (SEM), and Energy Dispersive X-ray (EDX) analysis. XRD analysis confirmed the crystalline nature of the nanoparticles, while DLS measurements revealed an average particle size of approximately 68.3 nm. FTIR spectra indicated the presence of functional groups associated with phytochemicals responsible for nanoparticle reduction and stabilization. UV–Vis spectroscopy confirmed the optical characteristics of the synthesized nanoparticles with calculated band gap energy of 2.71 eV. SEM micrographs demonstrated a distinctive clover-leaf-like morphology, and EDX analysis verified the elemental composition of titanium and oxygen. The biosynthesized nanoparticles exhibited promising pharmacological activities. The highest Antileishmanial activity reached 68%, anti-inflammatory activity 78%, and total antioxidant capacity (TAC) 79.1%. Furthermore, the nanoparticles showed notable antibacterial activity with a zone of inhibition (ZOI) of 22.1 mm, while a maximum growth inhibition of 85 ± 2.1% was observed against Ascochyta rabiei. In addition to their biomedical potential, the environmental application of the nanoparticles was evaluated for cadmium removal from aqueous solutions, achieving an adsorption efficiency of 85.3% within 120 min. Overall, the green-synthesized titanium dioxide nanoparticles demonstrated significant pharmacological and environmental potential. These findings highlight the promise of plant-mediated nanoparticle synthesis as a sustainable strategy for developing multifunctional nanomaterials with applications in biomedical and environmental remediation fields.

Keywords: Green synthesis; Phytofabrication; Titanium dioxide nanoparticles (TiO_2 NPs); *Acacia nilotica*; Antibacterial activity; Antileishmanial activity; Antioxidant activity; Environmental remediation; Cadmium adsorption

https://scientia-nexus.org/index.php/jpcs
DOI: https://doi.org/10.5281/zenodo.19767807

An Open-Access Peer-Reviewed Journal

1. Introduction

Nanotechnology has emerged as a rapidly expanding interdisciplinary field that integrates principles from chemistry, biology, physics, and materials science. The term "nano" refers to materials with dimensions ranging from 1 to 100 nm, which exhibit unique physicochemical and structural properties compared to their bulk counterparts. Due to their small size, large surface area, and enhanced reactivity, nanoparticles (NPs) have attracted significant attention for applications in medicine, environmental remediation, agriculture, and industrial technologies [1]. Nanoparticles can exist in various structural forms such as nanotubes, nanocrystals, nanowires, and nanoflowers, each possessing distinctive physical and chemical characteristics [2].

Among different nanomaterials, metal and metal oxide nanoparticles have gained considerable importance because of their high stability under extreme conditions such as elevated temperature and pressure, as well as their remarkable catalytic, optical, and biological properties. Commonly studied metal oxide nanoparticles include silver, zinc oxide, titanium dioxide, nickel oxide, calcium oxide, and iron oxide nanoparticles [3–8]. Some of these materials are considered relatively non-toxic and even contain elements essential for biological systems, making them promising candidates for applications in food packaging, healthcare, and environmental protection [9].

Conventional physical and chemical synthesis methods for nanoparticles often involve toxic chemicals, high energy consumption, and complex procedures that may generate hazardous by-products. Therefore, the development of environmentally friendly and sustainable synthesis routes has become an important focus of modern nanotechnology research. In this context, green synthesis approaches using biological resources have gained widespread attention [9]. Biological methods for nanoparticle synthesis include the use of microorganisms such as bacteria, fungi, and algae, as well as plant extracts [10–12]. Among these methods, plant-mediated synthesis has become particularly attractive because it is simple, cost-effective, rapid, and environmentally benign. Plant extracts contain diverse phytochemicals such as flavonoids, phenolics, terpenoids, and alkaloids, which can act as natural reducing and stabilizing agents during nanoparticle formation [13].

The plant-assisted synthesis of metal oxide nanoparticles has emerged as a sustainable strategy because the phytochemicals present in plant extracts facilitate both reduction and stabilization processes. These biomolecules can act as effective capping agents, stabilizing nanoparticles through steric interactions, electrostatic forces, and hydration effects, thereby improving their stability and biological activity [10]. Metal oxide nanoparticles synthesized through green routes have shown

https://scientia-nexus.org/index.php/jpcs
DOI: https://doi.org/10.5281/zenodo.19767807

An Open-Access Peer-Reviewed Journal

promising potential in fields such as nanomedicine, environmental remediation, and agriculture [14, 15].

Among various metal oxide nanoparticles, Titanium Dioxide (TiO_2) nanoparticles have attracted particular attention due to their excellent physicochemical properties, including high stability, optical transparency, photocatalytic activity, and non-toxic nature. In addition, TiO_2 nanoparticles are relatively inexpensive and widely available, making them highly suitable for large-scale applications [16, 17]. These nanoparticles have been extensively used in various industrial and biomedical applications such as catalysis, solar cells, coatings, paints, plastics, pharmaceuticals, and optoelectronic devices [18]. Moreover, TiO_2 nanoparticles are commonly incorporated in sunscreen formulations and cosmetic products due to their ability to effectively block ultraviolet radiation [19].

Recent studies have also demonstrated the strong antimicrobial potential of TiO_2 nanoparticles against various pathogenic microorganisms. These nanoparticles can interact with the phospholipid bilayer of microbial cell membranes, causing structural damage that ultimately leads to disruption of membrane integrity and microbial cell death [20, 21]. Consequently, TiO_2 nanoparticles are increasingly being explored as antimicrobial agents in medical materials, coatings, and environmental applications.

In addition to biomedical applications, environmental pollution has become a major global concern due to rapid industrialization and population growth. The discharge of industrial wastes into aquatic systems has led to the accumulation of toxic contaminants, including heavy metals, which pose severe threats to ecosystems and human health [22]. Heavy metals naturally occur in soil and water; however, their concentrations have increased significantly due to anthropogenic activities, resulting in serious environmental and health risks [23]. Among these contaminants, cadmium (Cd) is considered one of the most hazardous heavy metals because of its high toxicity and persistence in the environment [24].

Several conventional techniques have been employed for the removal of heavy metals from contaminated water, including chemical precipitation, ion exchange, membrane filtration, and adsorption processes [25–27]. However, these traditional methods often suffer from limitations such as high operational costs, high energy requirements, and the generation of secondary pollutants [28, 29]. Therefore, there is an urgent need to develop efficient, low-cost, and environmentally sustainable technologies for heavy metal removal.

In recent years, nano-based remediation strategies have emerged as promising alternatives for environmental purification. Due to their high surface area, enhanced adsorption capacity, and tunable surface properties, nanoparticles have demonstrated significant potential for the removal of

https://scientia-nexus.org/index.php/jpcs
DOI: https://doi.org/10.5281/zenodo.19767807

An Open-Access Peer-Reviewed Journal

toxic contaminants from water systems [30]. TiO_2 nanoparticles, in particular, have been widely investigated for heavy metal removal due to their small particle size, high adsorption capacity, and good biocompatibility [31, 32].

Medicinal plants also play an essential role in traditional and modern medicine due to their rich content of biologically active compounds. These phytochemicals contribute to various therapeutic activities such as antioxidant, antimicrobial, anti-inflammatory, and antidiabetic effects [33]. One such plant is *Acacia nilotica*, which is widely distributed in Pakistan and commonly used for medicinal, fuel, and wood production purposes [34]. Previous studies have reported that *A. nilotica* possesses several pharmacological properties, including analgesic, anti-platelet, antihyperglycemic, antioxidant, hepatoprotective, and antimicrobial activities [35–40].

Considering the growing demand for eco-friendly nanomaterials and sustainable environmental technologies, the present study focuses on the green synthesis of TiO_2 nanoparticles using *Acacia nilotica* leaf extract as a natural reducing and stabilizing agent. The synthesized nanoparticles were comprehensively characterized using various spectroscopic and microscopic techniques to investigate their structural and physicochemical properties. Furthermore, the biological and environmental applications of the synthesized nanoparticles were evaluated, including antibacterial, antioxidant, and anti-inflammatory activities, as well as their efficiency in removing cadmium from contaminated water. This research highlights the potential of plant-mediated TiO_2 nanoparticles as multifunctional nanomaterials for biomedical and environmental applications.

2. Materials and Methods

2.1: Chemicals

Titanium (IV) isopropoxide (TTIP) or titanium tetraisopropoxide ($Ti[OCH(CH_3)_2]_4$), sodium hydroxide (NaOH), dimethyl sulfoxide (DMSO), DPPH (2,2-diphenyl-1-picrylhydrazyl), methanol (CH_3OH), amphotericin-B, ascorbic acid, bovine serum albumin (BSA), Tris buffer, and diclofenac sodium were used in this study. Whatman filter paper No. 1 was used for filtration. All chemicals were purchased from Sigma-Aldrich (USA) and were of analytical grade. All reagents were used without further purification. The glassware used in the experiments was thoroughly washed with distilled water and sterilized prior to use [35].

https://scientia-nexus.org/index.php/jpcs
DOI: https://doi.org/10.5281/zenodo.19767807

An Open-Access Peer-Reviewed Journal

2. 2: Collection and Processing of Plant Samples

Fresh leaves of *Acacia nilotica* were collected from Jatoi, **Muzaffargarh, Punjab, Pakistan**. Plant collection was conducted following standard botanical guidelines. The plant specimen was identified by a qualified botanist and deposited in the herbarium with voucher number **Ak-2226**.

2.3: Preparation of Plant Extract

The collected leaves of *A. nilotica* were thoroughly washed with running tap water to remove dust and impurities. The leaves were then shade-dried at room temperature and ground into fine powder using an electric grinder. Approximately 10 g of powdered leaves was mixed with 250 mL of double-distilled water (DDW) and boiled for 15 min. The mixture was further incubated in a water bath at 80 °C for 15 min. After cooling to room temperature, the extract was filtered through muslin cloth followed by filtration using Whatman filter paper No. 1. The filtrate was stored at 4 °C for further use [36].

2.4: Qualitative Phytochemical Analysis

Qualitative phytochemical analysis was carried out to determine the presence of various bioactive compounds in the plant extract, including alkaloids, flavonoids, phenolics, glycosides, proteins, terpenoids, steroids, tannins, saponins, oils, quinones, and anthocyanins**.** The following standard phytochemical tests were used:

- **Mayer's test** – Alkaloids
- **Benedict's test** – Glycosides
- **Millon's test** – Proteins
- **Alkaline reagent test** – Flavonoids
- **Salkowski's test** – Steroids and terpenoids
- **Copper acetate test** – Phenolic compounds

The qualitative phytochemical screening was performed according to previously reported methods [1, 2].

https://scientia-nexus.org/index.php/jpcs
DOI: https://doi.org/10.5281/zenodo.19767807

An Open-Access Peer-Reviewed Journal

2.5: Synthesis of Titanium Dioxide Nanoparticles (TiO_2 NPs)

A 1 mM solution of titanium precursor (titanium tetraisopropoxide, TTIP) was prepared in distilled water. The previously prepared *Acacia nilotica* leaf extract was mixed with the titanium precursor solution in a 1:2 ratio under constant stirring. The reaction mixture was heated at 80 °C for 90 min using a magnetic stirrer. The reduction and formation of nanoparticles were indicated by a visible change in color of the reaction mixture. The mixture was then centrifuged at 6000 rpm for 35 min and washed several times with double-distilled water to remove impurities and unreacted compounds. The obtained pellet was dried in an incubator at 100 °C for 4 h to obtain a dry powder. The dried product was subsequently calcined at 600 °C for 2 h to obtain crystalline TiO_2 nanoparticles. The synthesized nanoparticles were further subjected to various physicochemical characterization techniques before evaluating their biological and environmental applications [37].

2.6: Characterization of TiO_2 Nanoparticles

2.6.1: UV–Visible Spectroscopy

The optical properties of the synthesized nanoparticles were analyzed using **UV–Visible spectroscopy**. The band gap energy of the nanoparticles was calculated using the Tauc relation:

$$(\alpha h\upsilon)2 = K(h\upsilon - Eg) \ldots\ldots\ldots\ldots\ldots\ldots\ldots\ldots\ldots (1)$$

Where α shows absorption coefficient, hυ represents photon energy (eV), K indicates absorption index and Eg is bandgap energy [38].

2.6.2: X-Ray Diffraction (XRD) Analysis

The crystalline structure of the synthesized nanoparticles was analyzed using X-ray diffraction **(XRD)**. The diffraction patterns were interpreted to determine crystal structure, diffraction planes, and lattice parameters.

The average crystallite size was calculated using the Scherrer equation:

$$D = \frac{0.9\lambda}{\beta cos\theta} \ldots\ldots\ldots\ldots\ldots\ldots\ldots\ldots\ldots (2)$$

Where D shows average crystalline size, λ represent X-Ray wavelength, β shows full width half maximum and θ shows diffraction angle.

https://scientia-nexus.org/index.php/jpcs
DOI: https://doi.org/10.5281/zenodo.19767807

An Open-Access Peer-Reviewed Journal

2.6.3: Fourier Transform Infrared Spectroscopy (FTIR)

FTIR analysis was performed to identify the functional groups present in the synthesized nanoparticles and to confirm the role of plant phytochemicals in nanoparticle stabilization. FTIR spectra were recorded following previously reported methods [39].

2.6.4: Scanning Electron Microscopy (SEM) and Energy Dispersive X-Ray (EDX) Analysis

The surface morphology and structural characteristics of the nanoparticles were examined using Scanning Electron Microscopy (SEM). Elemental composition and purity of the nanoparticles were determined using Energy Dispersive X-ray spectroscopy (EDX). These analyses confirmed the presence of titanium and oxygen elements in the synthesized nanoparticles.

2.6.5: Dynamic Light Scattering (DLS)

Dynamic Light Scattering (DLS) analysis was performed to determine the hydrodynamic particle size, polydispersity index (PDI), and zeta potential of the synthesized nanoparticles. Measurements were carried out following the previously reported method [4].

2.7: Biological Applications of TiO_2 Nanoparticles

2.7.1: Antileishmanial Activity

The antileishmanial activity of the synthesized nanoparticles was evaluated against *Leishmania tropica* promastigotes using a previously reported protocol.

Each assay tube contained 5 mL of culture medium with 1×10^5 parasites/mL**.** Different concentrations of nanoparticles (20, 40, 80, and 160 µg/mL) were added and incubated at 28 °C.

Amphotericin-B and DMSO were used as positive and negative controls, respectively. Parasite counts were measured using a hemocytometer after 24–96 h of incubation.

The percentage inhibition was calculated as:

$$(\%)\ Inhibition\ = \frac{Ab_{sample}}{Ab_{control}} \times 100 \quad \ldots\ldots\ldots\ldots\ldots\ldots\ldots\ldots\ldots (3)$$

In this, Ab_{sample} shows the absorbance of the TiO2 treated sample and $Ab_{control}$ mentions to the control sample.

2.7.2: Anti-Inflammatory Activity

The anti-inflammatory activity of plant extract and nanoparticles was evaluated using the protein denaturation inhibition assay [5]. Bovine serum albumin (BSA) solution was prepared in Tris buffer (pH 6.8). The reaction mixture consisted of:

https://scientia-nexus.org/index.php/jpcs
DOI: https://doi.org/10.5281/zenodo.19767807

An Open-Access Peer-Reviewed Journal

- 900 µL BSA solution
- 100 µL nanoparticle solution (50–800 µg/mL)

Diclofenac sodium was used as the standard drug. Absorbance was recorded at 580 nm. The percentage inhibition was calculated as:

$$Protein - Inhibition = Ab_{control} - Ab_{sample} \times 100 \quad \ldots\ldots\ldots\ldots\ldots\ldots\ldots\ldots\ldots (4)$$

2.7.3: Antioxidant Activities

The antioxidant potential of TiO_2 nanoparticles was evaluated using:

- Total antioxidant capacity (TAC)
- Total reducing power (TRP)
- DPPH free radical scavenging activity (FRSA)

The assays were performed at concentrations ranging from 50–200 µg/mL according to previously reported methods [6].

2.7.4: Total Antioxidant Capacity (TAC)

For TAC determination, **100 µL** of nanoparticle solution was mixed with the reaction reagent according to the standard method. Ascorbic acid and DMSO were used as positive and negative controls, respectively.

2.7.5: Total Reducing Power (TRP)

The reducing power assay was performed using the **potassium ferricyanide method** [7]. Absorbance was measured at **580 nm**.

2.7.6: Free Radical Scavenging Activity (FRSA)

DPPH free radical scavenging activity was determined using a standard method [6].

$$(\%)FRSA = \frac{Ab_{NPs-sample}}{Ab_{NPs-control}} \times 100 \quad \ldots\ldots\ldots\ldots\ldots\ldots\ldots (5)$$

2.8: Antimicrobial Activity

2.8.1: Antifungal Activity

The antifungal activity of the synthesized nanoparticles was tested against *Ascochyta rabiei* using the poisoned food technique.

https://scientia-nexus.org/index.php/jpcs
DOI: https://doi.org/10.5281/zenodo.19767807

An Open-Access Peer-Reviewed Journal

Potato dextrose agar (PDA) medium was supplemented with TiO_2 nanoparticles at concentrations of 0.5, 0.75, and 1 mg/mL. A 4 mm fungal disc was placed at the center of each Petri plate and incubated at 25 ± 1 °C for 7 days.

The percentage inhibition of fungal growth was calculated using:

$$Growth\ Inhibition\ \% = 100 \times \frac{C-T}{C} \ldots\ldots\ldots\ldots\ldots\ldots (6)$$

Where C refers to the fungus growth in the control plate, and T denotes to the fungus growth in a nanoparticle amended plate.

2.8.2: Antibacterial Activity

Antibacterial activity was evaluated against Escherichia coli using the agar well diffusion method. Different concentrations of nanoparticles (5, 10, and 20 mg/mL) were tested. Plates were incubated at 30 °C for 24 h, and the zone of inhibition (mm) was measured. Antibiotics and DMSO served as positive and negative controls, respectively.

2.9: Environmental Application: Cadmium Adsorption

The adsorption capability of TiO_2 nanoparticles was evaluated for the removal of cadmium (Cd) from aqueous solutions.

TiO_2 nanoparticles (1 g) were added to 100 mL of Cd solution (100 mg/L) in a 250 mL flask. The effect of various parameters such as:

- Initial Cd concentration (20–120 mg/L)
- Contact time (5–120 min)

was investigated. The mixture was shaken at 120 rpm at 25 °C.

Cd concentration was determined using an Atomic Absorption Spectrophotometer (AAS).

Adsorption capacity:

$$q_e = \frac{(C_i - C_e)V}{W} \ldots\ldots\ldots\ldots\ldots\ldots\ldots\ldots (7)$$

Adsorption efficiency:

https://scientia-nexus.org/index.php/jpcs
DOI: https://doi.org/10.5281/zenodo.19767807

An Open-Access Peer-Reviewed Journal

$$P = \frac{(C_i - C_e)}{C_i} \times 100 \ldots\ldots\ldots\ldots\ldots\ldots\ldots\ldots\ldots (8)$$

Where:

- **C_i** = initial concentration
- **C_e** = equilibrium concentration
- **V** = volume of solution
- **W** = mass of adsorbent

3. Results and Discussion (Integrated Summary)

3.1: Qualitative analysis of phytochemical

Qualitative assessment of extracts was accepted by analyzing phytochemicalcompoundsthatwerepresentindifferentpartsofplantsTable1.Thequalitativeanalysisof distilled water extracts of *A. nilotica* was carried out to detect the secondary metabolites like alkaloids, quinones, terpenoids, flavonoids, phenolic compounds, glycosides, saponins, steroids, anthocyanins, fats and oils, and tannins. These results are depicted in Table 1. There is a small variation in Qualitative phytochemical constituents were identified by previous researcher worked on *A. nilotica* [41], which may be due to the nature of the extract and plant physiological responses to their environment [42].

Table 1:

Sr. No	Secondary Metabolites	AMWD
1	Phenols	+++
2	Flavonoids	++
3	Alkaloids	++
4	Terpenoids	+
5	Saponins	-
6	Tannins	-

https://scientia-nexus.org/index.php/jpcs
DOI: https://doi.org/10.5281/zenodo.19767807

An Open-Access Peer-Reviewed Journal

7	Steroids	++
8	Glycosides	++
9	Quinones	+
10	Anthocynins	++
11	Fatsandoils	+
12	Protein	++

3.2: UV–Visible Spectroscopy

The successful formation of nanoparticles was confirmed using UV–visible spectroscopy through the observation of surface plasmon resonance (SPR). The plant extract exhibited an absorption peak at 225 nm (Figure 1a), whereas the synthesized TiO_2 nanoparticles (TiO_2 NPs) showed a characteristic absorption band around 350 nm (Figure 1b). During the synthesis process, the color of the cell-free culture changed from golden to creamy, providing an initial visual indication of nanoparticle formation. This color transformation is attributed to the reduction of the metal precursor by bioactive secondary metabolites present in the plant filtrate, which facilitate the conversion of the precursor into TiO_2 nanoparticles. Furthermore, the optical properties of the prepared nanomaterial were analyzed using UV–visible data, and the band gap energy was estimated to be approximately 2.71 eV. Similar absorption behavior has been reported for zinc oxide nanoparticles, which typically exhibit absorption peaks near 340 nm. Minor variations in the absorption maximum may arise due to differences in precursor materials, synthesis conditions, or particle size distribution [43].

Journal of Physical and Chemical Studies (JPCS), Volume 1, Issue 4 | April 2026 | pp. 17-56

https://scientia-nexus.org/index.php/jpcs
DOI: https://doi.org/10.5281/zenodo.19767807

An Open-Access Peer-Reviewed Journal

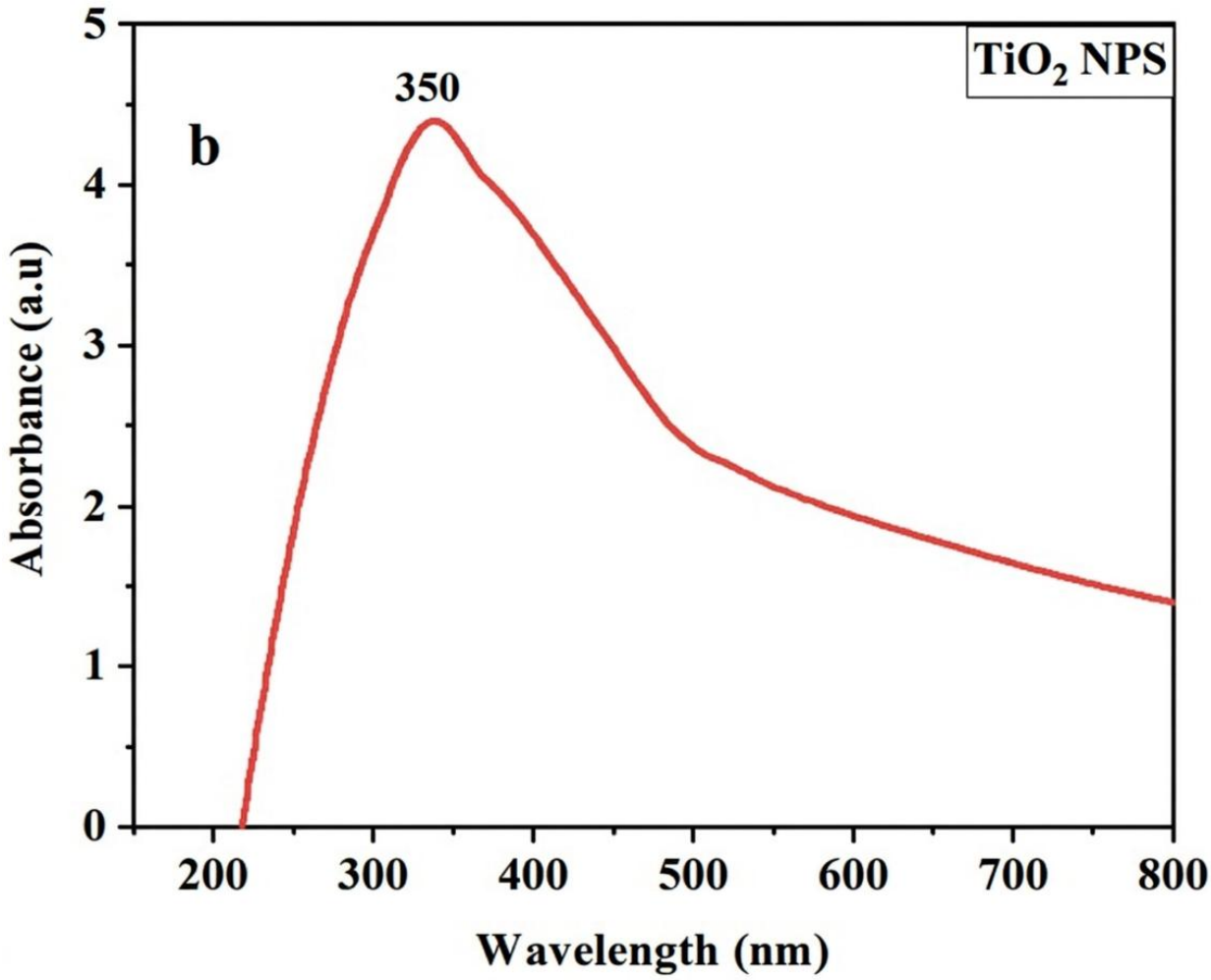

Figure1: UV-Vis spectroscopy of the prepared nanoparticles

3.3 Fourier Transform Infrared Spectroscopy (FTIR) Analysis

FTIR spectroscopy was used to identify the functional groups and confirm the TiO_2 lattice formation along with the surface functionalization that resulted from the green synthesis process. Figure 2 clearly shows that the strong, sharp characteristic absorption band observed at approximately 606 cm^{-1} is attributed to the antisymmetric O–Ti–O stretching vibration, confirming the successful formation of the TiO_2 crystal framework. Broad absorption around 3356 cm^{-1} and its shoulder near 1633 cm^{-1} correspond to O–H

https://scientia-nexus.org/index.php/jpcs
DOI: https://doi.org/10.5281/zenodo.19767807
An Open-Access Peer-Reviewed Journal

stretching and bending vibrations, respectively, which indicate the presence of adsorbed water molecules and surface hydroxyl (–OH) groups. These hydrophilic surface sites are conducive to the adsorption of aqueous pollutants and play an important role in enhancing the photocatalytic activity. The weaker bands in the 2800–3000 cm^{-1} region, noticeably around 2924 cm^{-1} and within 1379–1461 cm^{-1}, are assigned to C–H stretching and bending vibrations, respectively, arising from the residual organic moieties associated with plantderived phytochemicals acting as capping agents. The presence of these bioorganic surface groups contributes to the improvement in the dispersion of nanoparticles, the passivation of surface, and creation of more active sites for pollutant interaction. Overall, FTIR studies confirm the successful green synthesis of TiO_2 nanoparticles having a bio-functionalized surface chemistry that combines intrinsic metal–oxide bonding with organic capping layers, by which the material will be highly suitable for adsorption-based and photocatalytic environmental remediation applications [27-29].

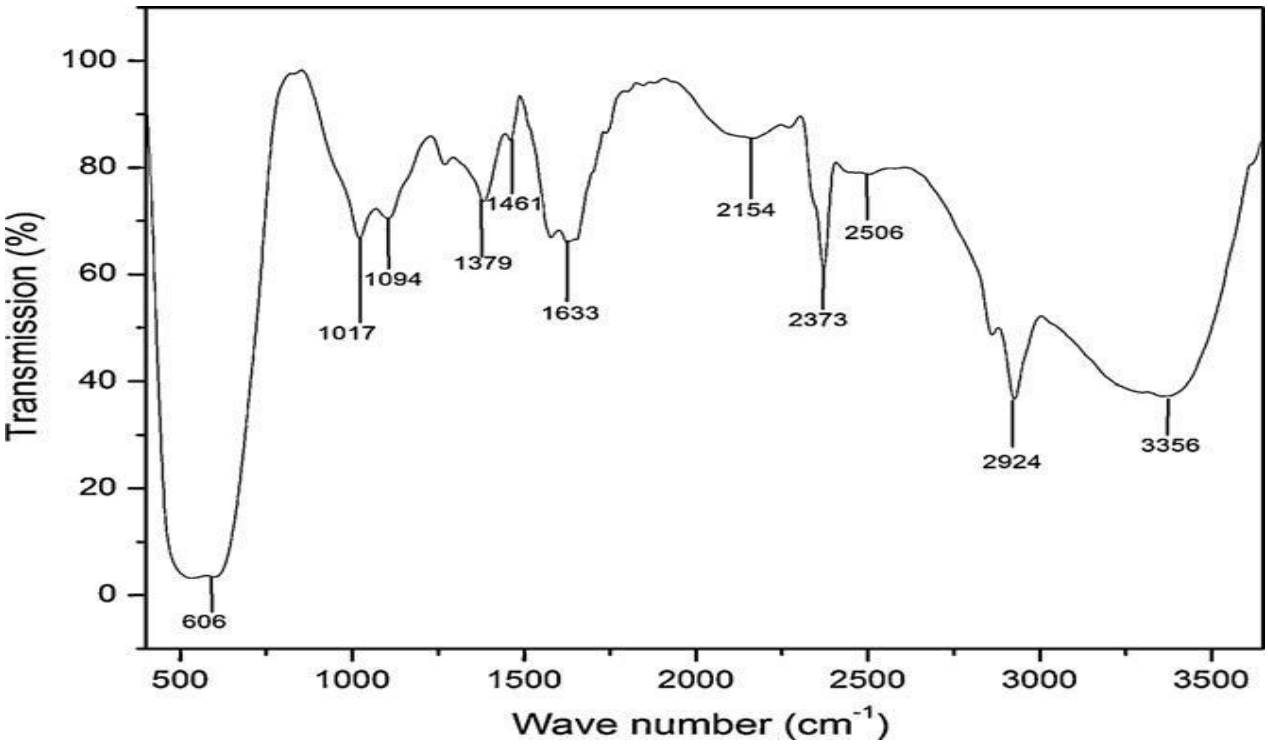

Figure 2: FTIR of green-synthesized TiO_2 nanomaterials.

Journal of Physical and Chemical Studies (JPCS), Volume 1, Issue 4 | April 2026 | pp. 17-56

https://scientia-nexus.org/index.php/jpcs
DOI: https://doi.org/10.5281/zenodo.19767807

An Open-Access Peer-Reviewed Journal

3.4 X-ray Diffraction (XRD) Analysis

The crystalline structure of the bio-fabricated TiO_2 nanoparticles (TiO_2 NPs) was examined using X-ray diffraction (XRD). The diffraction pattern exhibited several prominent peaks within the 2θ range of 10°–70°, with major reflections appearing at 32.5°, 34.1°, 37.5°, 48.1°, 56.3°, 63.5°, and 67.2° (Figure 2). These diffraction peaks correspond to the crystallographic planes (100), (002), (101), (102), (110), (103), (200), and (201), indicating a well-defined crystalline structure. The observed peaks were indexed according to the Joint Committee on Powder Diffraction Standards (JCPDS) database card No. 036-1451, confirming the formation of a hexagonal crystalline phase. The average crystallite size of the synthesized nanoparticles was estimated using the Debye–Scherrer equation, yielding an approximate particle size of 68.3 nm. Comparable findings have also been reported in previous studies [44]. The presence of sharp and intense diffraction peaks suggests the high crystallinity of the synthesized nanoparticles prepared using Acacia nilotica extract. The XRD results are consistent with earlier reports describing the crystalline nature of metal oxide nanoparticles [45]. It has been widely reported that the crystalline structure of nanoparticles significantly influences their physicochemical properties and biological performance [46]. Additionally, crystalline nanoparticles have been shown to exhibit enhanced antifungal activity, possibly due to their ability to disrupt fungal hyphal cell walls [36].

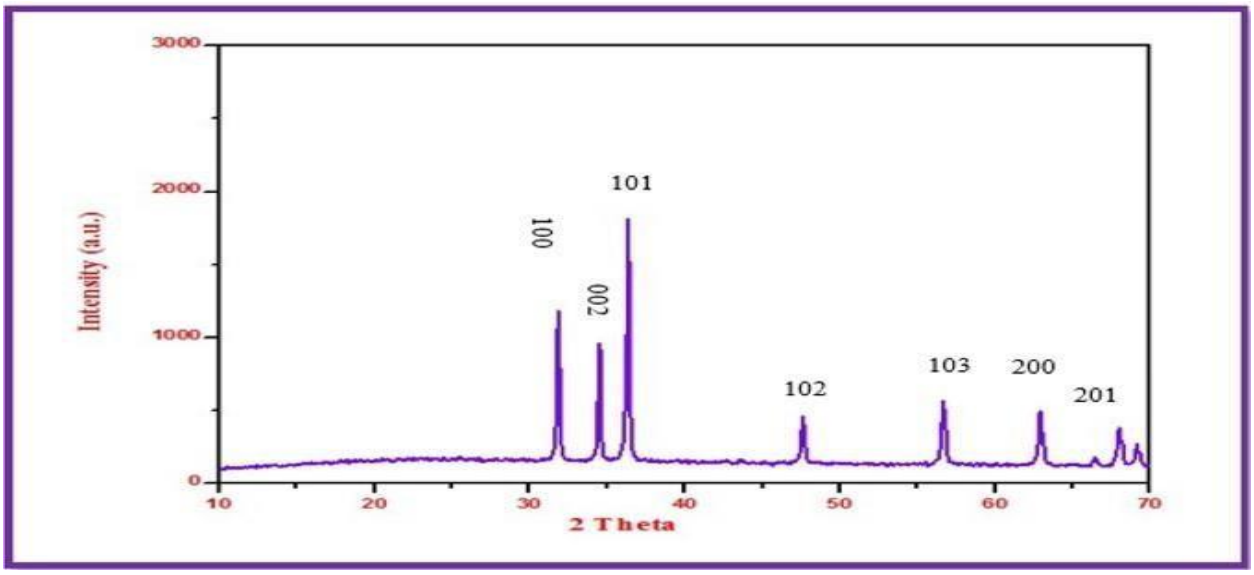

Figure 3: XRD pattern of the green synthesized TiO_2 nanoparticles.

Journal of Physical and Chemical Studies (JPCS), Volume 1, Issue 4 | April 2026 | pp. 17-56

https://scientia-nexus.org/index.php/jpcs
DOI: https://doi.org/10.5281/zenodo.19767807

An Open-Access Peer-Reviewed Journal

3.5 Scanning Electron Microscopy (SEM) and Energy Dispersive X-ray (EDX) Analysis

Scanning Electron Microscopy (SEM) was employed to investigate the surface morphology, texture, and distribution of the synthesized TiO_2 nanoparticles (TiO_2 NPs). The morphological characteristics of the prepared nanoparticles are presented in Figure 4a. The SEM micrograph reveals that the TiO_2 nanoparticles appear as white, cotton-like agglomerates with clover-leaf shaped structures, distributed relatively uniformly across the surface. The homogeneous distribution of nanoparticles provides valuable insight into their morphological characteristics and allows an approximate estimation of particle size. Similar morphological observations have also been reported in previous studies [13]. Overall, the SEM results are consistent with earlier reports on biosynthesized metal oxide nanoparticles [14].

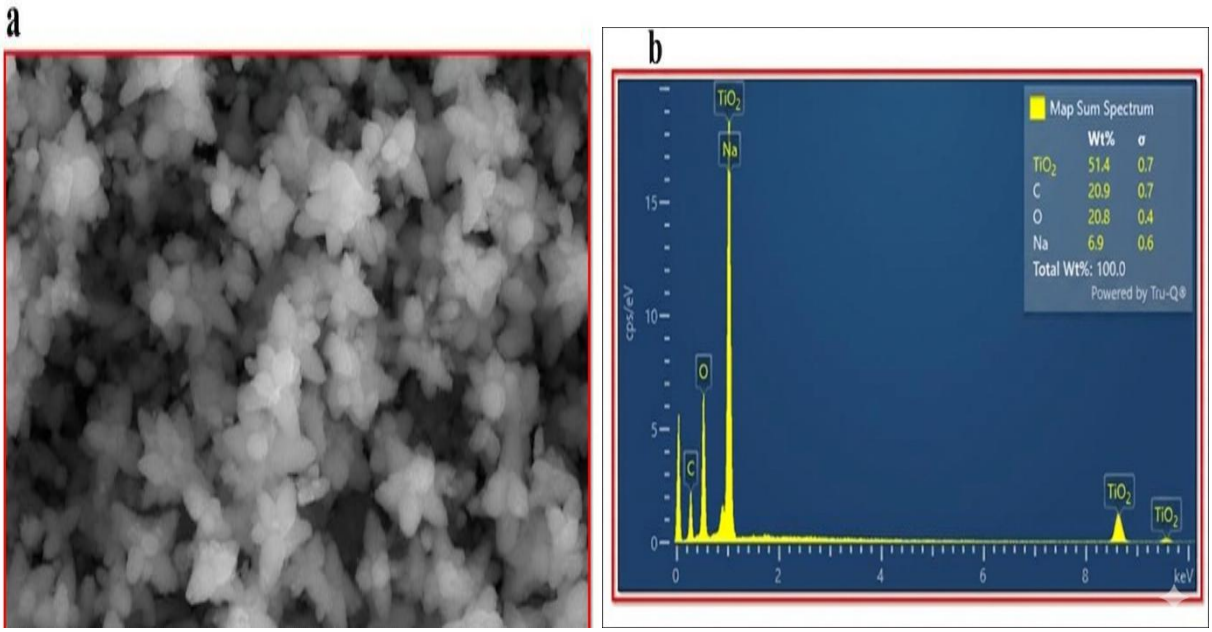

Figure 4. SEM (a) and EDX (b) of the prepared nanoparticles

The elemental composition and chemical configuration of the synthesized nanoparticles were further analyzed using Energy Dispersive X-ray spectroscopy (EDX). The EDX spectrum (Figure 4b) confirmed the presence of the principal elements associated with the nanoparticles, along with additional elements originating from the plant extract used during the green synthesis process. The

https://scientia-nexus.org/index.php/jpcs
DOI: https://doi.org/10.5281/zenodo.19767807

An Open-Access Peer-Reviewed Journal

detected elements included zinc (Zn) and oxygen (O) as major components, while carbon (C) and sodium (Na) were also observed with weight percentages of 20.8% and 6.9%, respectively. The relatively high carbon content is likely attributed to organic biomolecules present in the plant extract, which act as reducing and stabilizing agents during nanoparticle synthesis. The measured weight percentages of Zn and O were 51.4% and 20.8%, respectively, confirming the formation of metal oxide nanoparticles. These observations are in agreement with previously reported studies on green synthesized nanoparticles [34]. Furthermore, elemental mapping using EDS was performed to examine the spatial distribution of elements within the sample. The elemental distribution image (Figure 5) demonstrates that the nanoparticles are well dispersed across the carbon support film. The rapid detection and clear elemental distribution confirm the efficiency of the EDS detector for the identification and mapping of the synthesized nanoparticles.

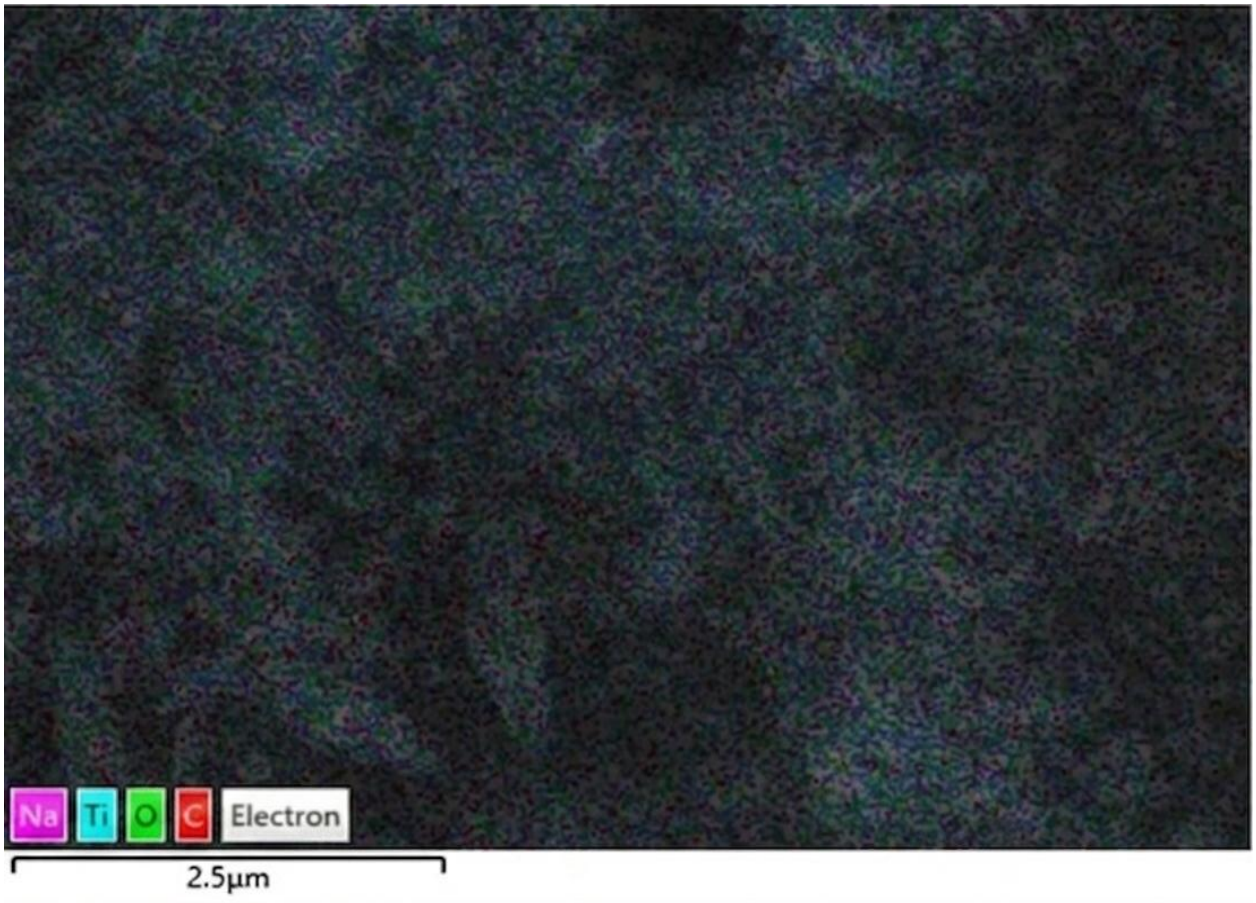

Figure 5. EDS analysis of the prepared nanoparticles.

https://scientia-nexus.org/index.php/jpcs
DOI: https://doi.org/10.5281/zenodo.19767807

An Open-Access Peer-Reviewed Journal

3.6: Zeta Potential (ZP) Analysis

Zeta potential (ZP) analysis was performed to determine the surface charge and colloidal stability of the synthesized TiO_2 nanoparticles (TiO_2 NPs). The zeta potential measurement reflects the electrical potential at the nanoparticle surface, which plays an important role in determining the stability of nanoparticle suspensions. The electrostatic repulsion between neighboring particles in a colloidal system can be evaluated through the zeta potential value. Nanoparticle suspensions with zeta potential values in the range of +8.50 to −8.50 mV generally indicate a moderate level of stability due to electrostatic interactions between particles (Sarkar et al., 2014). In the present study, the synthesized TiO_2 nanoparticles exhibited a zeta potential value of −8.95 mV (Figure 6a), indicating the presence of a negatively charged nanoparticle surface. Figure 6b illustrates the particle size distribution and light scattering intensity obtained from dynamic light scattering (DLS) measurements. The average hydrodynamic diameter of the TiO_2 nanoparticles was found to be 663.5 nm, with a polydispersity index (PDI) of 0.523, suggesting moderate size distribution within the suspension. Previous studies on plant- and algae-mediated nanoparticle synthesis have also reported negative zeta potential values [24]. The negative surface charge is typically attributed to the adsorption of plant-derived secondary metabolites and biomolecules onto the nanoparticle surface [36]. In the present study, the negative zeta potential of the plant-mediated TiO_2 nanoparticles may be associated with the binding of phytochemical constituents that act as reducing and stabilizing agents during nanoparticle synthesis [37].

Journal of Physical and Chemical Studies (JPCS), Volume 1, Issue 4 | April 2026 | pp. 17-56

https://scientia-nexus.org/index.php/jpcs
DOI: https://doi.org/10.5281/zenodo.19767807

An Open-Access Peer-Reviewed Journal

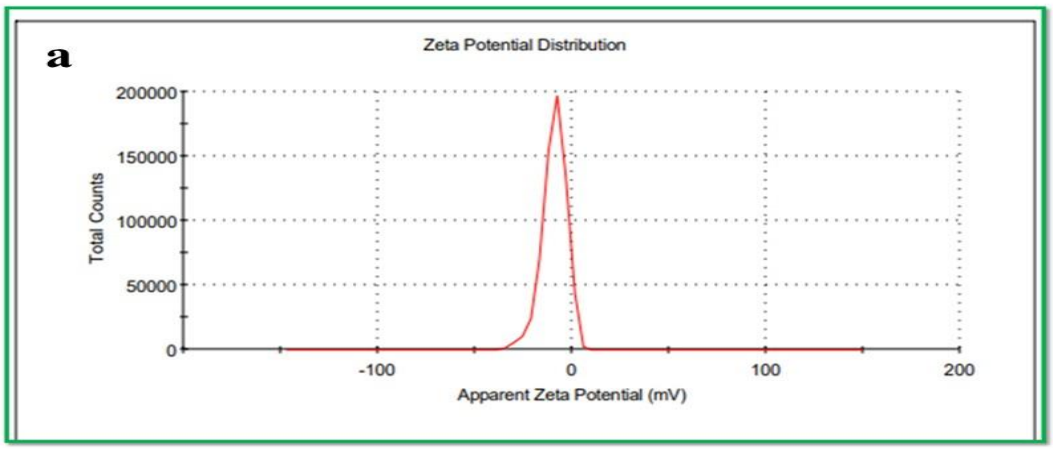

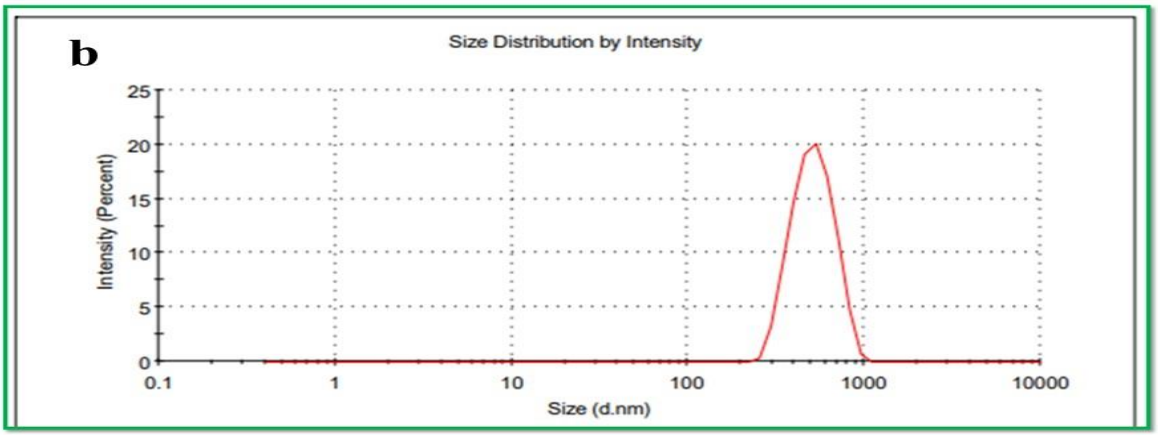

Figure 6. Zeta potential (a) and light scattering intensity with particle size distribution (b) of the synthesized TiO_2 nanoparticles.

3.7 Antileishmanial Activity

The antileishmanial activity of the synthesized TiO_2 nanoparticles (TiO_2 NPs) was evaluated by exposing Leishmania promastigotes to different nanoparticle concentrations for a period of 96

https://scientia-nexus.org/index.php/jpcs
DOI: https://doi.org/10.5281/zenodo.19767807

An Open-Access Peer-Reviewed Journal

hours. The results of the assay are illustrated in Figure 7. To determine the antileishmanial potential, the number of promastigotes was counted in both NP-treated and control groups at different time intervals, including 24, 48, 72, and 96 hours. The results demonstrated that the antileishmanial activity increased with increasing concentrations of TiO_2 nanoparticles. After 24 hours of incubation, the inhibition percentages were 20%, 30%, 32%, and 37% at concentrations of 20, 40, 80, and 160 µg/mL, respectively. After 48 hours, the inhibitory effect further increased to 27%, 32%, 39%, and 48% at the same concentrations. Following 72 hours of incubation, a further reduction in promastigote numbers was observed in the TiO_2 NP-treated samples, showing 35% inhibition at 20 µg/mL, 48% at 40 µg/mL, 60% at 80 µg/mL, and 68% at 160 µg/mL. However, after prolonged exposure, a slight decrease in antileishmanial activity was observed.

The observed inhibitory effect may be associated with the generation of reactive oxygen species (ROS) by TiO_2 nanoparticles. Metal oxide nanoparticles are known to produce reactive ions and oxidative stress, which can disrupt the cell membrane integrity of pathogens, leading to the formation of pores in the cell wall, leakage of intracellular components, and ultimately cell death. The findings of the present study suggest that TiO_2 nanoparticles possess promising antileishmanial properties, indicating their potential as a novel nanomaterial-based therapeutic approach for leishmaniasis treatment. These results are consistent with previously reported studies on nanoparticle-mediated antimicrobial activity [25].

Journal of Physical and Chemical Studies (JPCS), Volume 1, Issue 4 | April 2026 | pp. 17-56

https://scientia-nexus.org/index.php/jpcs
DOI: https://doi.org/10.5281/zenodo.19767807

An Open-Access Peer-Reviewed Journal

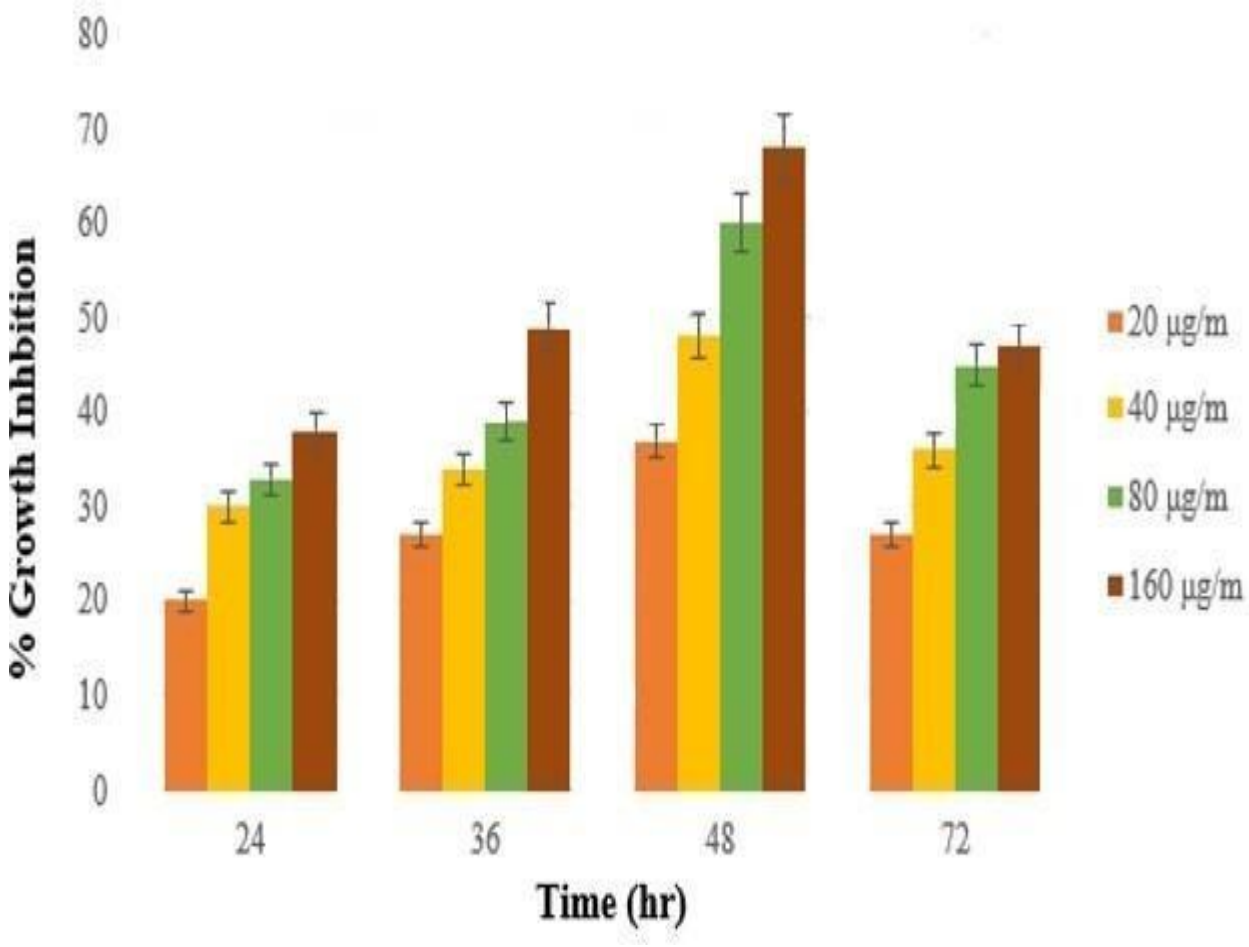

Figure 7. Antileishmanial Activity of the Prepared Nanoparticles

3.8 Anti-Inflammatory Potential

The anti-inflammatory activity of the synthesized TiO_2 nanoparticles (TiO_2 NPs) and the plant extract of Acacia nilotica was evaluated and compared with the standard anti-inflammatory drug diclofenac sodium. The results indicated that both the plant extract and the synthesized nanoparticles exhibited significant anti-inflammatory effects, as illustrated in Figure 8. The plant-mediated TiO_2 nanoparticles demonstrated enhanced anti-inflammatory activity compared with the plant extract alone. Both samples were effective in reducing in vitro inflammation, but the

Journal of Physical and Chemical Studies (JPCS), Volume 1, Issue 4 | April 2026 | pp. 17-56

https://scientia-nexus.org/index.php/jpcs
DOI: https://doi.org/10.5281/zenodo.19767807

An Open-Access Peer-Reviewed Journal

nanoparticle formulation showed higher inhibition levels. The maximum anti-inflammatory activity of TiO_2 nanoparticles was observed as 45% inhibition at 50 µg/mL, 58% at 100 µg/mL, 65% at 200 µg/mL, 70% at 400 µg/mL, and 78% at 800 µg/mL. However, further increases in concentration beyond 800 µg/mL did not result in a significant increase in inhibition, indicating a plateau in anti-inflammatory activity. A comparative analysis revealed that TiO_2 nanoparticles exhibited stronger anti-inflammatory potential than the plant extract alone. Previous studies have also reported that plant-mediated nanoparticles possess superior anti-inflammatory properties compared with chemically or physically synthesized nanoparticles, as well as crude plant extracts used in anti-inflammatory treatments [12].

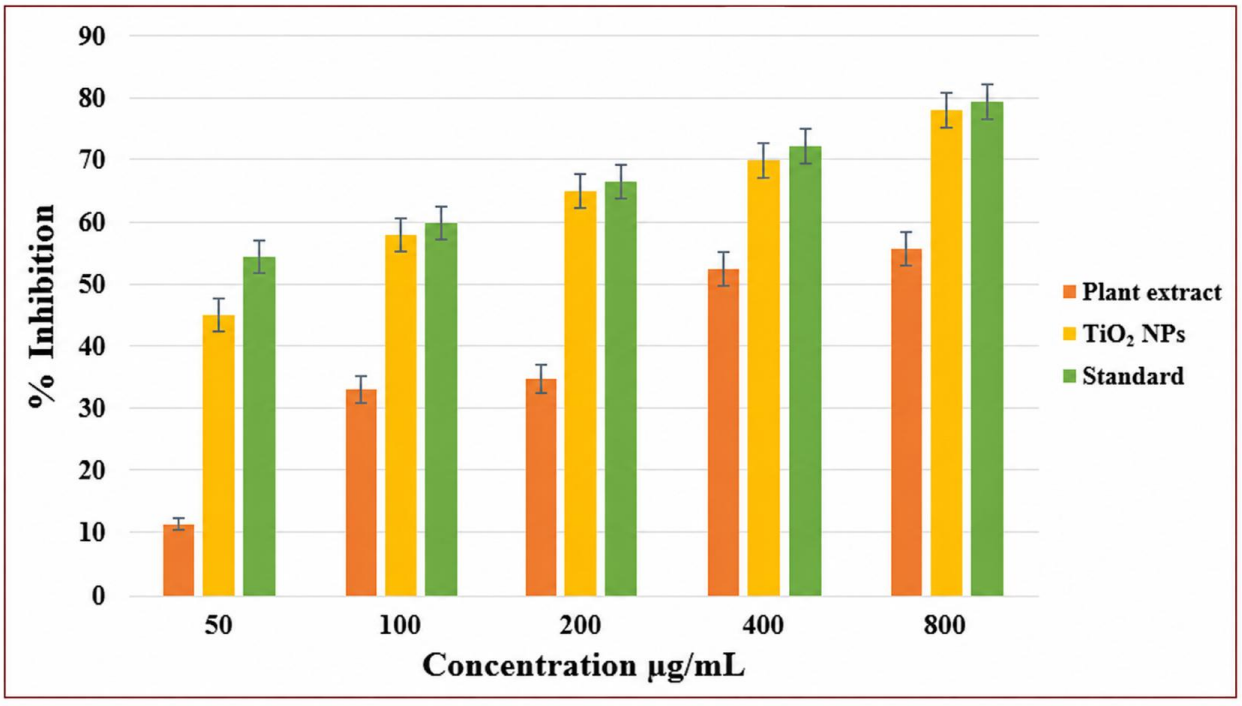

Figure 11: Anti-Inflammatory potential of the Prepared Nanoparticles

https://scientia-nexus.org/index.php/jpcs
DOI: https://doi.org/10.5281/zenodo.19767807

An Open-Access Peer-Reviewed Journal

3.9 Antioxidant Assay

The antioxidant activity of the synthesized TiO_2 nanoparticles (TiO_2 NPs) was evaluated at different concentrations ranging from 50 to 2000 µg/mL. The antioxidant potential was determined using total antioxidant capacity (TAC), total reducing power (TRP), and DPPH free radical scavenging assays, as illustrated in Figure 9. The maximum total antioxidant capacity (TAC), expressed as ascorbic acid (AA) equivalents per mg, was observed to be 79.1% at a concentration of 200 µg/mL for TiO_2 nanoparticles. The TAC assay demonstrates the ability of TiO_2 NPs to neutralize reactive oxygen species (ROS) through their free radical scavenging properties. The total reducing power (TRP) assay was further conducted to evaluate the presence of antioxidant compounds associated with the nanoparticles. This assay measures the ability of reductones to donate electrons, which plays a significant role in antioxidant activity (Siripireddy et al., 2017). The highest TRP value of 65.2% was recorded at 200 µg/mL. Similarly, the DPPH free radical scavenging assay indicated strong antioxidant activity of the synthesized nanoparticles. The maximum DPPH radical scavenging activity was 68.7% at a concentration of 2000 µg/mL [27]. Overall, the results demonstrate that plant-mediated TiO_2 nanoparticles possess considerable antioxidant potential, which may be attributed to the bioactive phytochemicals attached to the nanoparticle surface during green synthesis. These findings are consistent with previous reports on bio-inspired TiO_2 nanoparticles and their antioxidant properties [28-30].

Journal of Physical and Chemical Studies (JPCS), Volume 1, Issue 4 | April 2026 | pp. 17-56

https://scientia-nexus.org/index.php/jpcs
DOI: https://doi.org/10.5281/zenodo.19767807

An Open-Access Peer-Reviewed Journal

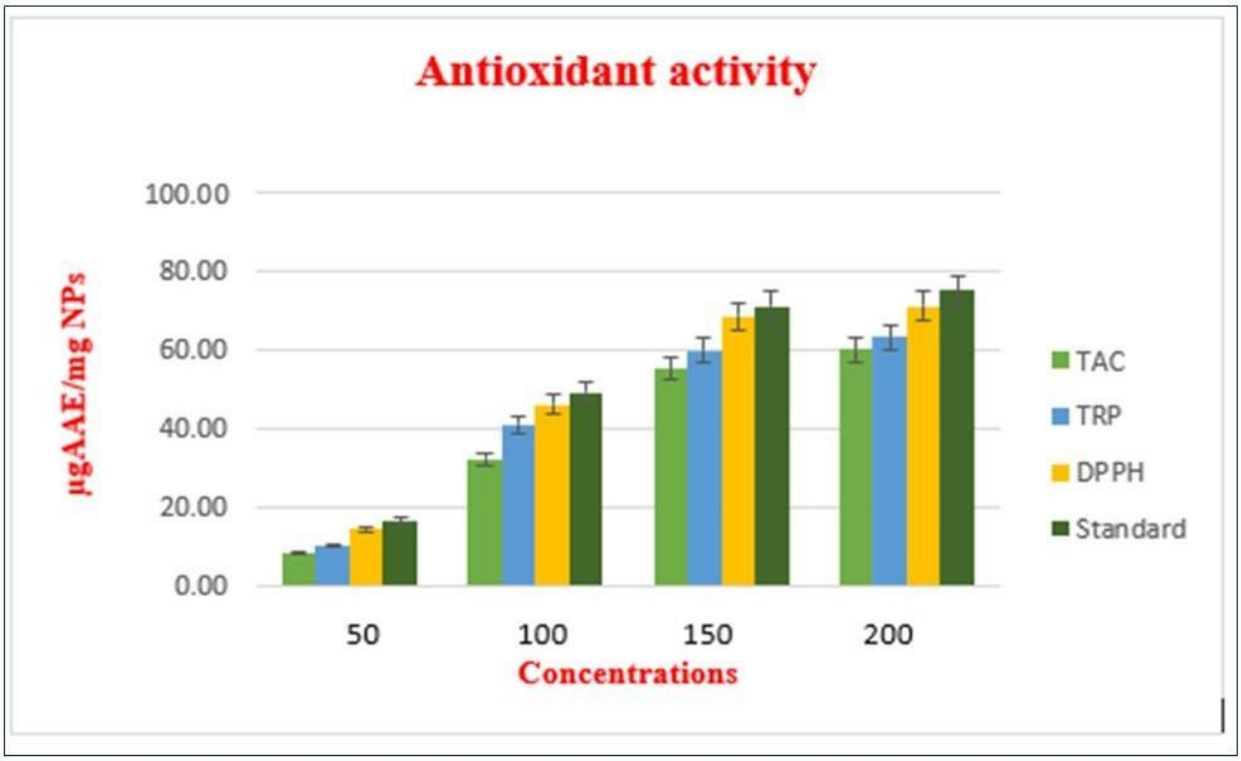

Figure 12: Antioxidant activity of the prepared nanoparticles

3.10 In Vitro Antibacterial Assay

In the present study, Escherichia coli (E. coli) was used as a model organism to evaluate the antibacterial activity of the synthesized TiO_2 nanoparticles (TiO_2 NPs). The antibacterial potential of the prepared nanoparticles is illustrated in Figure 10a–d. For this purpose, 100 µL of different nanoparticle concentrations (5, 10, and 20 mg/mL) were applied against E. coli, and the zone of inhibition (ZOI) was measured to determine antibacterial efficacy.

The results demonstrated a concentration-dependent antibacterial activity of TiO_2 nanoparticles. The maximum zone of inhibition (22.1 mm) was observed at a concentration of 20 mg/mL, followed by 17.4 mm at 10 mg/mL and 10.2 mm at 5 mg/mL (Figure 10a–d). A comparison of the antibacterial activity of the synthesized nanoparticles with previously reported studies is presented in Table 2. The bacterial cell membrane acts as the primary protective barrier against external antimicrobial agents. Nanoparticles, particularly metal oxide nanoparticles, possess a large surface-

https://scientia-nexus.org/index.php/jpcs
DOI: https://doi.org/10.5281/zenodo.19767807

An Open-Access Peer-Reviewed Journal

to-volume ratio, which enhances their interaction with bacterial cells and facilitates the generation of reactive oxygen species (ROS). These reactive species can damage cellular components, including proteins, lipids, and DNA, leading to bacterial cell death [20].

Previous studies have reported that TiO_2 nanoparticles exhibit bactericidal effects rather than bacteriostatic effects, as no recovery of bacterial cells was observed after treatment (Al Rugaie et al., 2022). The antibacterial mechanism is believed to involve membrane damage, pore formation, and leakage of intracellular components. The internalization of TiO_2 nanoparticles can disrupt the phospholipid bilayer, resulting in the release of intracellular substances such as lipopolysaccharides and ATP, ultimately leading to bacterial cell death [32].

Furthermore, nanoparticle interaction with bacterial membranes may cause membrane depolarization by interfering with ion channels such as K^+ channels, thereby disturbing the normal physiological functions of the bacterial cell [33]. Changes in zeta potential of the bacterial surface can also serve as an indicator of membrane damage [35]. Additionally, nanoparticle exposure may induce lipid peroxidation and oxidative stress, further contributing to bacterial inhibition [37]. Overall, the results of the present study demonstrate that the antibacterial activity increases with increasing concentrations of TiO_2 nanoparticles, which is consistent with previously reported findings [39].

Journal of Physical and Chemical Studies (JPCS), Volume 1, Issue 4 | April 2026 | pp. 17-56

https://scientia-nexus.org/index.php/jpcs
DOI: https://doi.org/10.5281/zenodo.19767807

An Open-Access Peer-Reviewed Journal

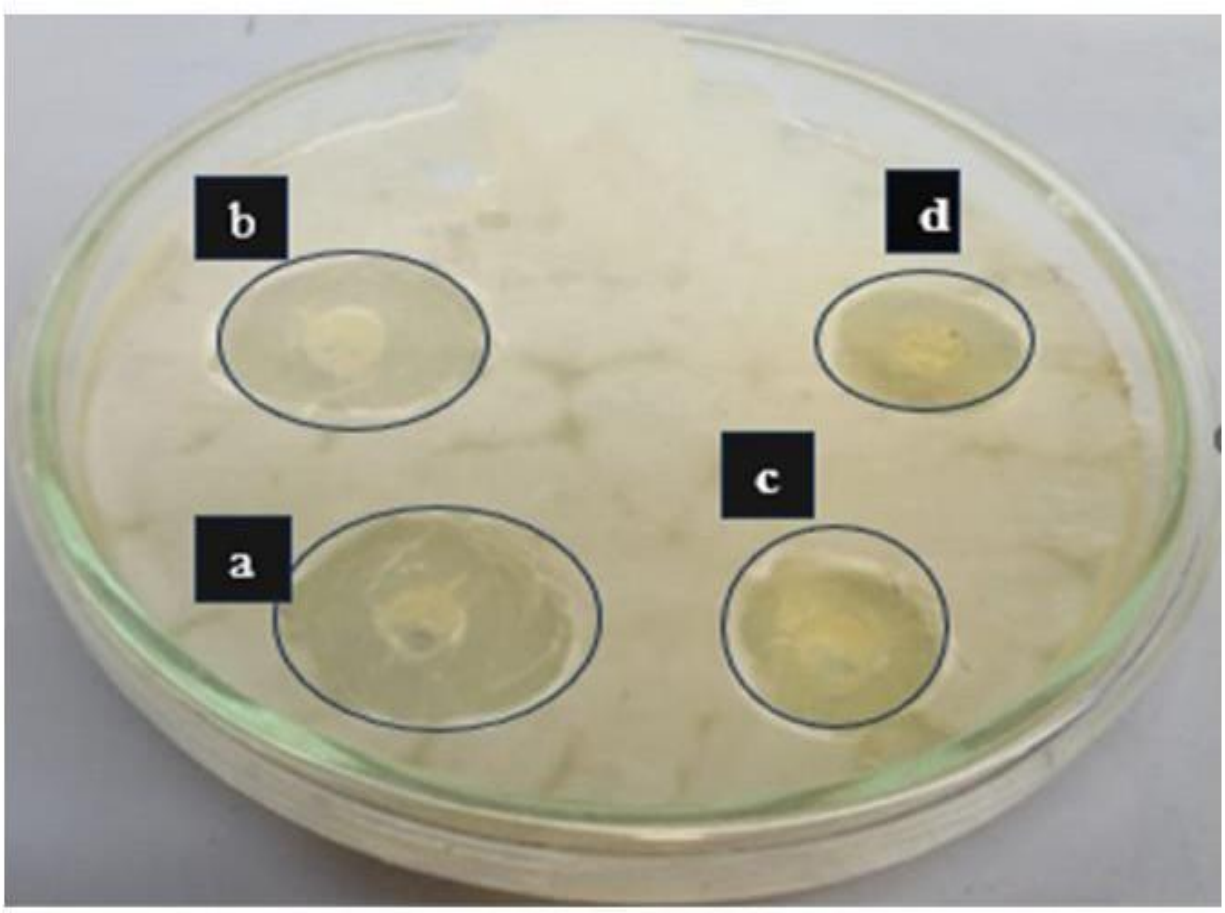

Figure13: Antibacterialactivity of the TiO_2 NPs

Table 2. Comparative antibacterial activity of TiO_2 nanoparticles with previously reported studies

Nanoparticles / Study	Test Organism	Method	Zone of Inhibition (mm) / Activity	Reference
Plant-mediated TiO_2 NPs (*A. nilotica*)	*E. coli*	Agar well diffusion	10.2 mm (5 mg/mL), 17.4 mm (10 mg/mL), 22.1 mm (20 mg/mL)	Present study

https://scientia-nexus.org/index.php/jpcs
DOI: https://doi.org/10.5281/zenodo.19767807

An Open-Access Peer-Reviewed Journal

Green synthesized TiO_2 NPs	*E. coli*	Agar diffusion	18–21 mm	Yin et al., 2023
Biosynthesized TiO_2 NPs	*Campylobacter jejuni*	Culture inhibition	Strong bactericidal effect	Al Rugaie et al., 2022
Metal oxide nanoparticles	*E. coli*	Antibacterial assay	Significant ROS-mediated inhibition	Muthuvel et al., 2020
Bio-inspired TiO_2 nanoparticles	Gram-negative bacteria	Disc diffusion	Enhanced antibacterial activity	Zhang et al., 2023

3.11. Antifungal Assay

The antifungal activity of the synthesized TiO_2 nanoparticles (TiO_2 NPs) was evaluated using potato dextrose agar (PDA)–supplemented Petri plates, and the results are presented in Figure 11a–d. The antifungal efficacy was assessed by measuring the percentage inhibition of fungal growth at different nanoparticle concentrations. The results indicated a dose-dependent inhibition of fungal growth. The highest growth inhibition (85 ± 2.1%) was observed at a concentration of 1 mg/mL, followed by 66 ± 1.7% inhibition at 0.75 mg/mL and 56.77 ± 0.5% inhibition at 0.50 mg/mL. However, a further increase in nanoparticle concentration did not significantly enhance antifungal activity. This behavior may be attributed to the agglomeration of nanoparticles at higher concentrations, which reduces their effective surface area and interaction with fungal cells.

Nanoparticles possess small particle size and a high surface-to-volume ratio, which enhances their reactivity and stability [44]. In addition, physicochemical properties such as particle size, Brownian motion, and surface charge may influence nanoparticle aggregation and interaction with fungal cells. Over the past decade, TiO_2 nanoparticles have been widely reported to inhibit the growth of various fungal pathogens, including Fusarium graminearum, Candida albicans, and Aspergillus niger [45]. Previous studies suggest that the antifungal activity of metal oxide nanoparticles is mainly associated with the generation of reactive oxygen species (ROS). These reactive species can damage cellular components and disrupt fungal metabolism. Furthermore, nanoparticles can strongly interact with the fungal cell wall and plasma membrane, leading to membrane depolarization and altered membrane permeability [46]. Metal oxide nanoparticles may create pores in the fungal cell wall, which disrupts the structural integrity of the membrane and allows nanoparticles to penetrate into the cytoplasm. This penetration results in the damage of intracellular biomolecules such as DNA, RNA, proteins, and enzymes, ultimately causing fungal cell death [31].

https://scientia-nexus.org/index.php/jpcs
DOI: https://doi.org/10.5281/zenodo.19767807

An Open-Access Peer-Reviewed Journal

The proposed mechanism of antimicrobial activity of TiO_2 nanoparticles is illustrated in Figure 11.

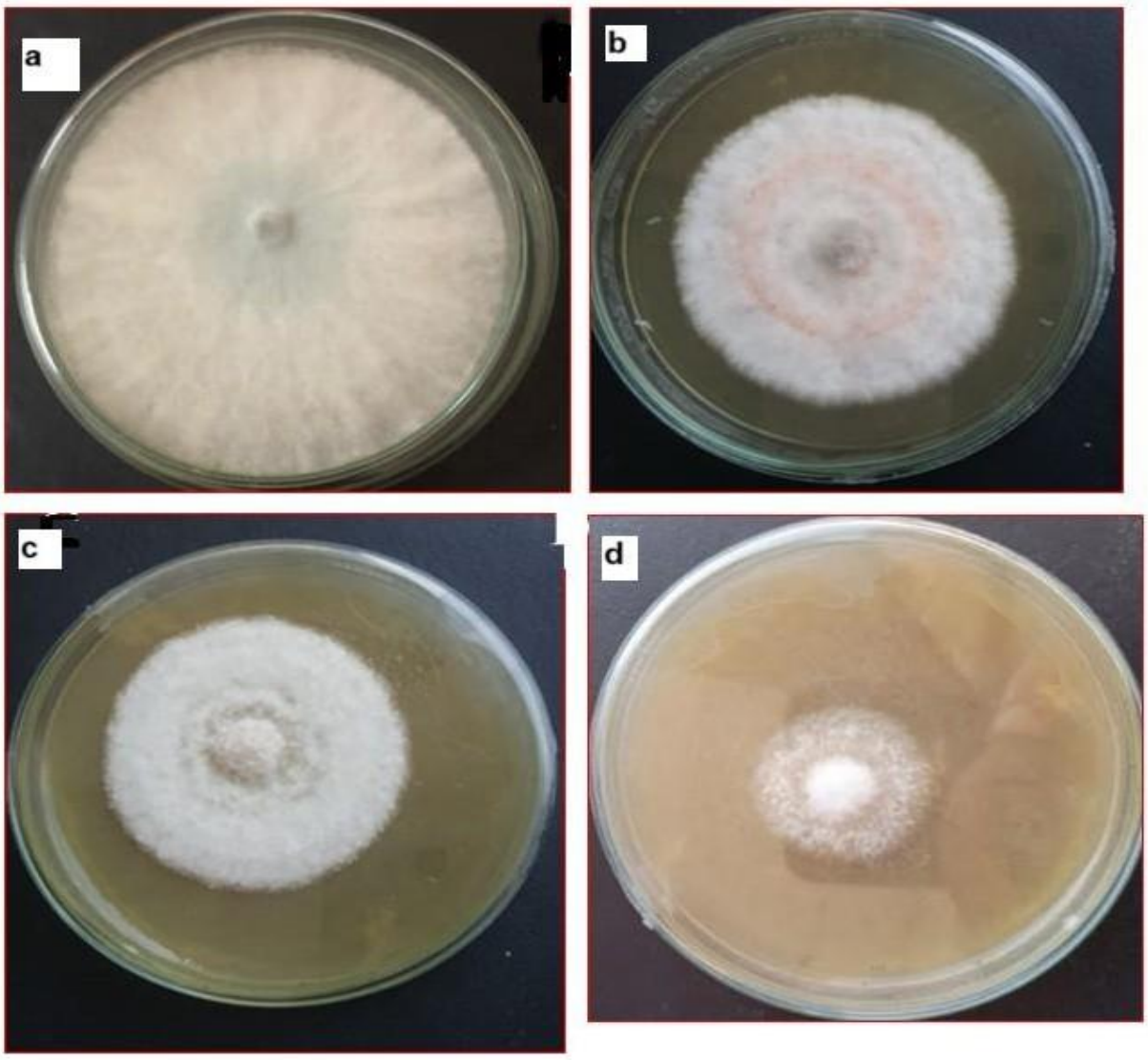

Figure14: Antibacterial activity of the TiO_2 NPs

Journal of Physical and Chemical Studies (JPCS), Volume 1, Issue 4 | April 2026 | pp. 17-56

https://scientia-nexus.org/index.php/jpcs
DOI: https://doi.org/10.5281/zenodo.19767807

An Open-Access Peer-Reviewed Journal

4. Assessment of TiO_2 Nanoparticles in Cd Adsorption

4.1 Effect of Contact Time and Adsorption Kinetics

Contact time is an important factor in the adsorption of metal ions by nanosorbents during wastewater treatment. Adsorption refers to the accumulation of solutes or sorbates at the surface or interface of solid materials [32]. Therefore, a comprehensive investigation was carried out to examine the effect of contact time on the adsorption process over a period ranging from 5 to 120 minutes. At the initial stage, the adsorption rate was relatively high, as illustrated in Figure 13. This rapid uptake may be attributed to the presence of abundant active adsorption sites on the surface of TiO_2 nanoparticles [26-29]. As the contact time between Cd ions and TiO_2 nanoparticles increased, the adsorption efficiency improved significantly due to enhanced interaction between Cd ions and the available active sites. The maximum adsorption capacity of 85.3 mg/g was observed at a contact time of 120 minutes. These results demonstrate that TiO_2 nanoparticles possess strong adsorption capability and can serve as an effective adsorbent for the removal of Cd ions from aqueous solutions. Similar findings have been reported in earlier studies on pollutant removal using nanomaterials [35].

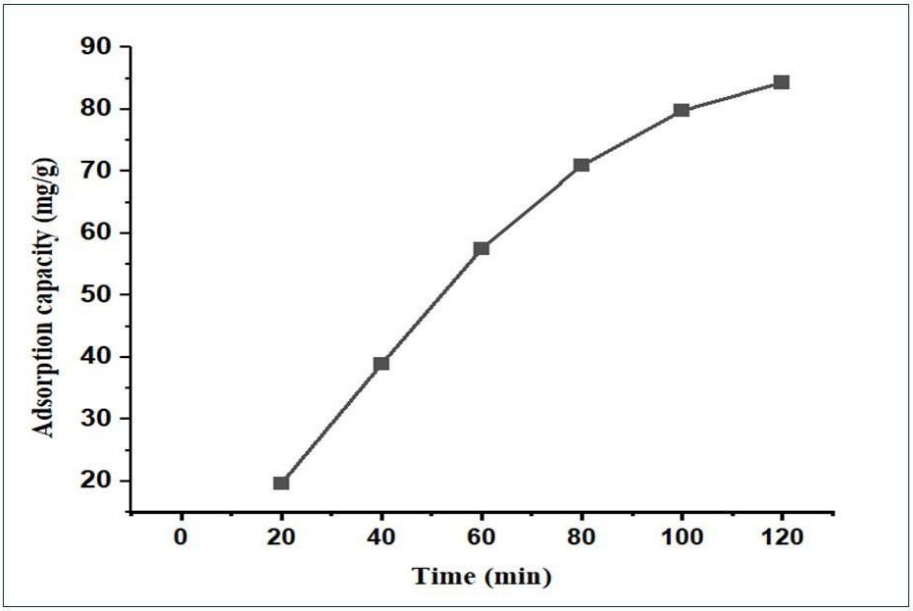

Figure 15: Adsorption rate of Cd ions using TiO_2 nanoparticles.

https://scientia-nexus.org/index.php/jpcs
DOI: https://doi.org/10.5281/zenodo.19767807

An Open-Access Peer-Reviewed Journal

A kinetic study is a fundamental approach for evaluating the efficiency of adsorption processes in environmental remediation. In this study, adsorption kinetics of Cd ions onto TiO_2 nanoparticles were analyzed using two widely applied kinetic models: the pseudo-first-order kinetic model (P1stOK) and the pseudo-second-order kinetic model (P2ndOK), as illustrated in Figure 13a and 13b. The pseudo-first-order kinetic model assumes that adsorption occurs through weak interactions between TiO_2 nanoparticles and Cd ions, primarily governed by physisorption forces [2]. The linear form of the pseudo-first-order equation is expressed as:

$$\ln(qe-qt)=\ln qe-K1t$$

where (qt) represents the amount of Cd adsorbed at time (t), and (qe) is the amount of Cd adsorbed at equilibrium. The rate constant of the pseudo-first-order model is denoted as (K1) (min^{-1}). The kinetic parameters were determined by plotting ln(qe – qt) versus time (t).

The pseudo-second-order kinetic model, on the other hand, assumes that adsorption is mainly governed by chemisorption mechanisms involving electron sharing or exchange between the adsorbent and adsorbate [16]. The mathematical form of this model is expressed as:

$$\frac{t}{qt} = \frac{1}{K2\ qe2} + \frac{t}{qe}$$

The rate constant (K2) was determined by plotting t/qt versus t.

A significantly higher correlation coefficient (R^2) was obtained for the pseudo-second-order model compared to the pseudo-first-order model, confirming that the adsorption kinetics of Cd onto TiO_2 nanoparticles are better described by the pseudo-second-order model (Table 6). This finding suggests that chemisorption is the rate-limiting step in the adsorption process. These results are consistent with previously reported studies [18-22].

Journal of Physical and Chemical Studies (JPCS), Volume 1, Issue 4 | April 2026 | pp. 17-56

https://scientia-nexus.org/index.php/jpcs
DOI: https://doi.org/10.5281/zenodo.19767807

An Open-Access Peer-Reviewed Journal

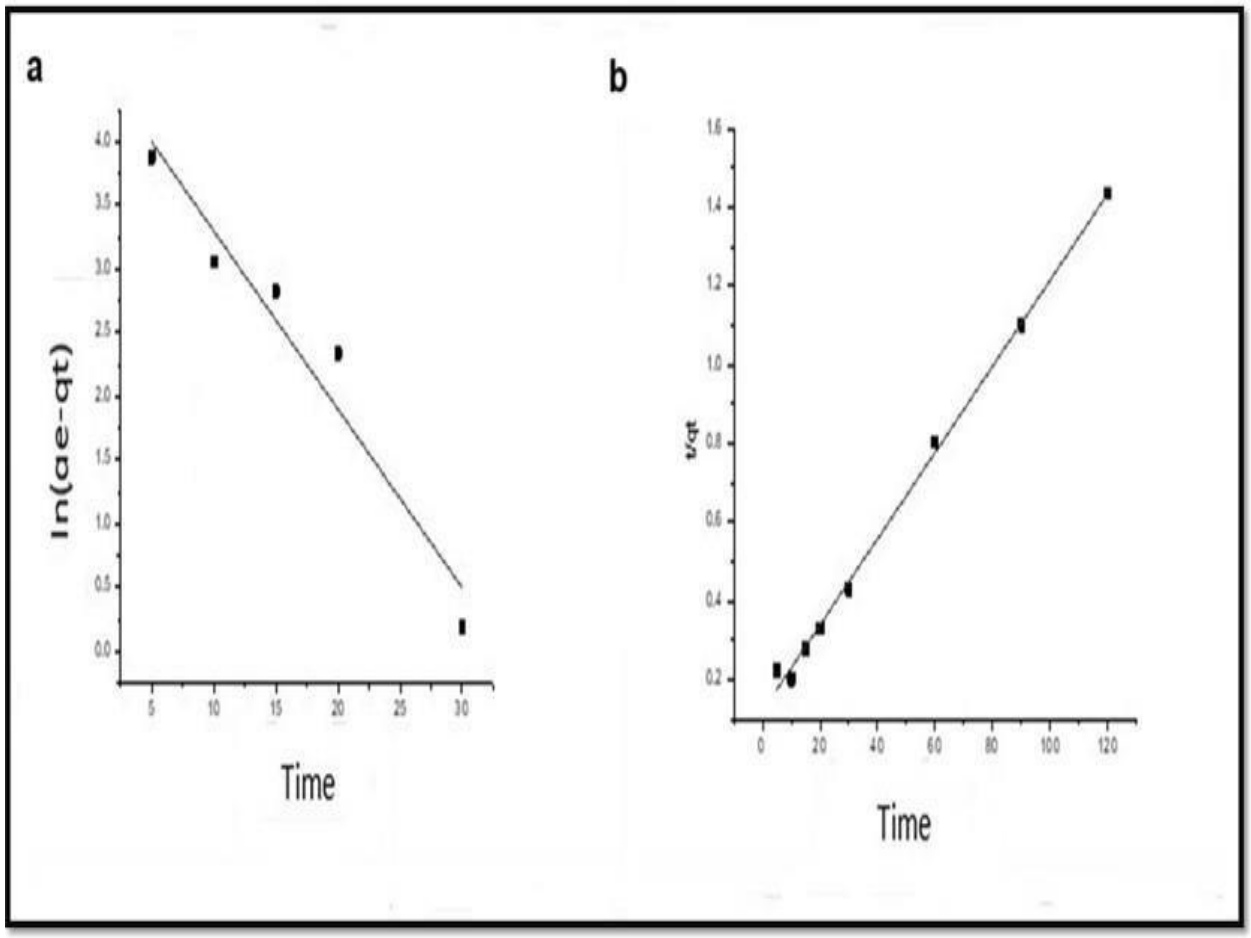

Figure 16: Evaluation of adsorption mechanism using kinetic models.

4.2. Effect of Initial Metal Concentration on Adsorption

The influence of the initial concentration of Cd ions on adsorption by TiO_2 nanoparticles was investigated at concentrations ranging from 20 to 120 mg/L, as presented in Figure 14. The results indicated that Cd adsorption increased with increasing initial metal concentration. The maximum adsorption capacity (80.3 mg/g) was observed at the highest Cd concentration of 120 mg/L. The enhancement in adsorption capacity with increasing metal concentration may be attributed to the higher availability of Cd ions in the solution, which increases the probability of interaction with active adsorption sites on the nanoparticles. These results are consistent with previous studies on

Journal of Physical and Chemical Studies (JPCS), Volume 1, Issue 4 | April 2026 | pp. 17-56

https://scientia-nexus.org/index.php/jpcs
DOI: https://doi.org/10.5281/zenodo.19767807

An Open-Access Peer-Reviewed Journal

metal ion adsorption using organic and nanomaterial-based adsorbents (Ameh et al., 2023; Dubey et al., 2016).

One of the main objectives of this study was to apply Langmuir and Freundlich isotherm models to evaluate the adsorption behavior of Cd ions on TiO_2 nanoparticles.

The Langmuir isotherm model describes adsorption occurring on a homogeneous surface with the formation of a monolayer of adsorbate molecules when equilibrium is reached between the solid and liquid phases (Ho & McKay, 1998). The linear form of the Langmuir equation is expressed as:

$$\frac{1}{qe} = \frac{1}{KL\ qmax\ Ce} + \frac{1}{qmax}$$

where (KL) represents the Langmuir constant, (qmax) is the maximum adsorption capacity, and (Ce) is the equilibrium concentration of the metal ions. The **separation factor (RL)** is given by:

$$RL = \frac{1}{1 + Ci\ KL}$$

The **Freundlich isotherm model**, on the other hand, describes **multilayer adsorption on heterogeneous surfaces** [2]. The Freundlich equation is expressed as:

$$log\ qe = log\ Kf + \frac{1}{n}\ log\ Ce$$

where (Kf) represents the Freundlich constant and (1/n) indicates the adsorption intensity.

The isotherm plots are shown in Figures 13a and 13b, while the calculated isotherm parameters and correlation coefficients are summarized in Table 3. The results demonstrate that the Langmuir model exhibits a higher correlation coefficient (R^2) than the Freundlich model, indicating that the Langmuir model better describes the adsorption of Cd ions onto TiO_2 nanoparticles. This suggests that the adsorption process occurs predominantly as monolayer adsorption on a homogeneous surface.

The maximum adsorption capacity calculated from the Langmuir model was 85.69 mg/g, indicating strong adsorption potential of TiO_2 nanoparticles. Additionally, the Freundlich parameter (1/n) was found to be 0.3013, which lies between 0 and 1, confirming that the adsorption process is favorable [5-13]. Overall, the results suggest that the adsorption process closely follows the Langmuir isotherm model.

Journal of Physical and Chemical Studies (JPCS), Volume 1, Issue 4 | April 2026 | pp. 17-56

https://scientia-nexus.org/index.php/jpcs
DOI: https://doi.org/10.5281/zenodo.19767807

An Open-Access Peer-Reviewed Journal

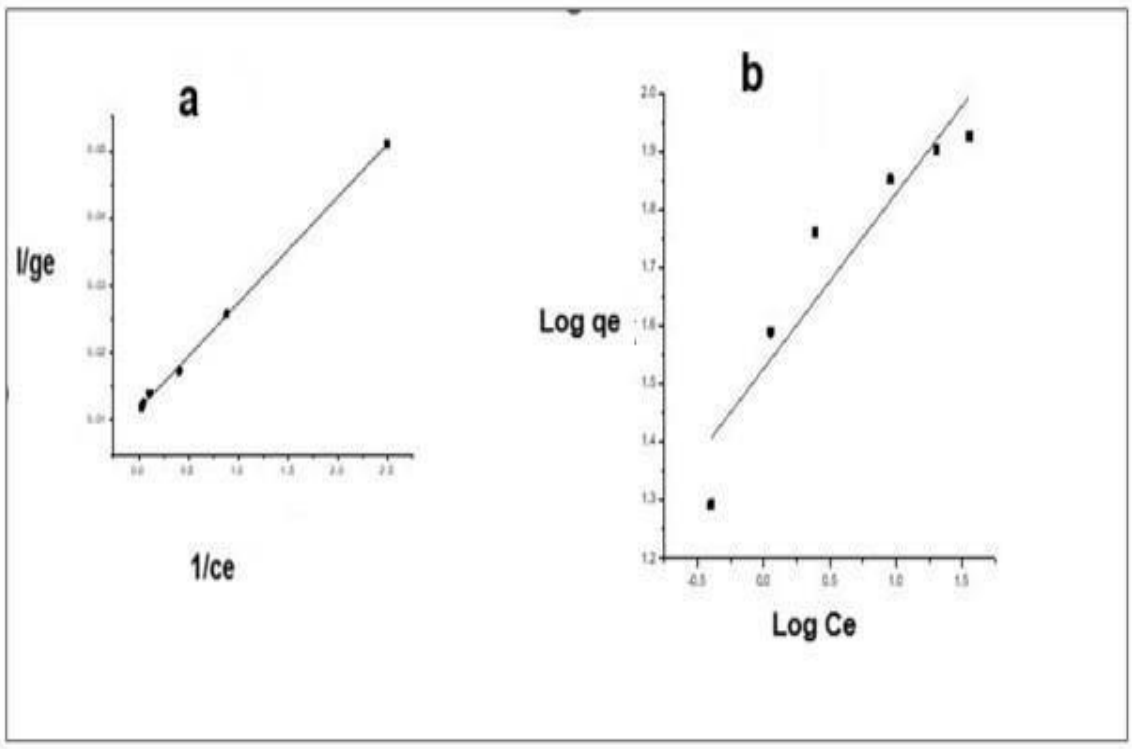

Figure 17: Effect of initial Cd concentration on adsorption by TiO_2 nanoparticles.

Table 3. Kinetic parameters for Cd adsorption onto TiO_2 nanoparticles

Kinetic Model	Parameter	Value
Pseudo-First-Order Model (P1stOK)	qe (mg g^{-1})	63.42
	k_1 (min^{-1})	0.018
	R^2	0.921
Pseudo-Second-Order Model (P2ndOK)	qe (mg g^{-1})	85.30
	k_2 (g mg^{-1} min^{-1})	0.0027
	R^2	0.992

https://scientia-nexus.org/index.php/jpcs
DOI: https://doi.org/10.5281/zenodo.19767807

An Open-Access Peer-Reviewed Journal

Table 4. Langmuir and Freundlich isotherm parameters for Cd adsorption onto TiO_2 nanoparticles

Isotherm Model	Parameter	Value
Langmuir Isotherm	qmax (mg g^{-1})	85.689
	KL (L mg^{-1})	0.043
	RL	0.162
	R^2	0.991
Freundlich Isotherm	Kf (mg g^{-1})(L mg^{-1})$^{1}/^{n}$	21.74
	1/n	0.3013
	R^2	0.948

5. Conclusion

Interest in green nanotechnology has increased significantly due to the demand for non-toxic, cost-effective, and environmentally friendly materials. In the present study, TiO_2 nanoparticles (TiO_2 NPs) were successfully synthesized through an eco-friendly green synthesis approach using Acacia nilotica leaf extract as a reducing and stabilizing agent. The synthesized nanoparticles were thoroughly characterized using various microscopic and spectroscopic techniques, confirming their successful formation and structural properties.

The prepared TiO_2 nanoparticles demonstrated promising performance in biomedical and environmental applications. The nanoparticles exhibited significant antioxidant, antibacterial, antifungal, anti-inflammatory, and antileishmanial activities, indicating their potential for various biomedical uses. Furthermore, the synthesized TiO_2 nanoparticles showed excellent adsorption capability for cadmium (Cd) ions, highlighting their potential application in environmental remediation and wastewater treatment.

Overall, the results of this study suggest that bio-fabricated TiO_2 nanoparticles represent a promising candidate for both biological and environmental applications, particularly for the removal of toxic chemicals and heavy metals from contaminated water and sewage systems. Notably, the synthesis method employed in this study is green, sustainable, and free from hazardous chemicals, making it environmentally safe and economically feasible.

https://scientia-nexus.org/index.php/jpcs
DOI: https://doi.org/10.5281/zenodo.19767807

An Open-Access Peer-Reviewed Journal

Despite these encouraging findings, several challenges still need to be addressed. Future research should focus on developing more sustainable synthesis strategies, improving nanoparticle stability, enhancing targeted delivery in biomedical applications, and minimizing potential toxicity to human health and the environment. Additionally, interdisciplinary collaboration among scientists, engineers, and policymakers will be essential to fully exploit the potential of nanotechnology in addressing global environmental and healthcare challenges. By overcoming current limitations and leveraging the opportunities offered by nanomaterials, a more sustainable and technologically advanced future can be achieved.

Competing Interests

There are no conflicts of interest exist among authors of this research paper.

ACKNOWLEDGEMENTS

Author Contributions

M.A.A wrote the main manuscript Draft, writing, studied Data validation and Editing, Reviewing. All authors reviewed the manuscript outline.

Funding

No external fundings.

Data Availability

No data sets were generated or analysed during the current study.

6. References

1. Dijoo, Z. K., & Khurshid, R. (2022). Environmental degradation as a multifaceted consequence of human development. In *Environmental Biotechnology* (pp. 39-56). Apple Academic Press.
2. Saxena, V. (2025). Water quality, air pollution, and climate change: investigating the environmental impacts of industrialization and urbanization. *Water, Air, & Soil Pollution*, *236*(2), 73.
3. Ganivet, E. (2020). Growth in human population and consumption both need to be addressed to reach an ecologically sustainable future. *Environment, Development and Sustainability*, *22*(6), 4979-4998.

https://scientia-nexus.org/index.php/jpcs
DOI: https://doi.org/10.5281/zenodo.19767807

An Open-Access Peer-Reviewed Journal

4. Akhtar, M. S., Ali, S., & Zaman, W. (2024). Innovative adsorbents for pollutant removal: exploring the latest research and applications. *Molecules*, *29*(18), 4317.
5. Rath, P., Jindal, M., & Jindal, T. (2021). A review on economically-feasible and environmental-friendly technologies promising a sustainable environment. *Cleaner Engineering and Technology*, *5*, 100318.
6. Haq, I., & Kalamdhad, A. S. (2022). Advanced and Ecofriendly Technologies for the Treatment of Industrial Wastewater to Constrain Environmental Pollution. In *Innovations in Environmental Biotechnology* (pp. 561-573). Singapore: Springer Nature Singapore.
7. Bharagava, R. N. (Ed.). (2020). *Emerging eco-friendly green technologies for wastewater treatment*. Berlin, Heidelberg, Germany: Springer.
8. Singh, V., Ahmed, G., Vedika, S., Kumar, P., Chaturvedi, S. K., Rai, S. N., ... & Kumar, A. (2024). Toxic heavy metal ions contamination in water and their sustainable reduction by eco-friendly methods: isotherms, thermodynamics and kinetics study. *Scientific Reports*, *14*(1), 7595.
9. Shamshad, J., & Rehman, R. U. (2025). Innovative approaches to sustainable wastewater treatment: a comprehensive exploration of conventional and emerging technologies. *Environmental Science: Advances*.
10. Zahan, M. S., Munshi, M. R., Rana, M. Z., & Al Masud, M. (2023). Theoretical insights on geometrical, mechanical, electronic, thermodynamic and photocatalytic characteristics of RaTiO3 compound: a DFT investigation. *Computational Condensed Matter*, *36*, e00832.
11. Manikandan, I., Perumal, M. V., & Jayamoorthy, K. (2019). Synthesis, characterization, physico-chemical and DFT studies of potential organic NLO materials: experimental and theoretical combined study. *Silicon*, *11*(1), 425-435.
12. Ahmed, T. Y., Aziz, S. B., & Dannoun, E. M. (2024). New photocatalytic materials based on alumina with reduced band gap: A DFT approach to study the band structure and optical properties. *Heliyon*, *10*(5).
13. Ullah, H. N., Rizwan, M., Zahid, U., Imran, A., & Cao, C. (2022). A comprehensive DFT study of physical and photocatalytic properties of Sr1-xCdxTiO3. *Materials Today Communications*, *33*, 104495.
14. Hassan, A. U., Sumrra, S. H., Zubair, M., Mustafa, G., Noreen, S., & Imran, M. (2023). Correlating the charge density and structural fabrication of new organic dyes to create

https://scientia-nexus.org/index.php/jpcs
DOI: https://doi.org/10.5281/zenodo.19767807

An Open-Access Peer-Reviewed Journal

visible light harvesting materials with tunable NLO refining: insights from DFT. *Chemical Papers*, *77*(10), 6183-6202.

15. Khan, W., Tariq, A., Minar, J., Durrani, S., Raziq, A., Azam, S., & Saeed, K. (2025). Band structure engineering, optical, transport, and photocatalytic properties of pristine and doped Nb 3 O 7 (OH): a systematic DFT study. *RSC advances*, *15*(4), 2452-2460.
16. Latif, A., Latif, A., Mohsin, M., & Bhatti, I. A. (2025). Density functional theory for nanomaterials: structural and spectroscopic applications—a review. *Journal of Molecular Modeling*, *31*(8), 211.
17. Lalithambika, K. C., Shanmugapriya, K., & Sriram, S. J. A. P. A. (2019). Photocatalytic activity of MoS2 nanoparticles: an experimental and DFT analysis. *Applied Physics A*, *125*(12), 817.
18. Zhao, Y., Zhang, S., Shi, R., Waterhouse, G. I., Tang, J., & Zhang, T. (2020). Two-dimensional photocatalyst design: A critical review of recent experimental and computational advances. *Materials Today*, *34*, 78-91.
19. Hamad, H., Elsenety, M. M., Sadik, W., El-Demerdash, A. G., Nashed, A., Mostafa, A., & Elyamny, S. (2022). The superior photocatalytic performance and DFT insights of S-scheme CuO@ TiO2 heterojunction composites for simultaneous degradation of organics. *Scientific reports*, *12*(1), 2217.
20. Abbas, M. A., Mahar, J., Hameed, N., & Rasool, M. S. (2025). DFT-Guided Design of a Low-Band-Gap Pyrazoline Scaffold: The Critical Role of a Para-Nitro Substituent. *Multidisciplinary Surgical Research Annals*, *3*(3), 461-503.
21. Abbas, M. A., Mahar, J., Rasool, M. S., Khan, M. J., & Khan, M. Z. (2025). The Dual Therapeutic Promise of Quinoa: Exploring Antidiabetic and Antioxidant Effects through Experimental and Computational Models. *Multidisciplinary Surgical Research Annals*, *3*(3), 504-544.
22. Abbas, M. A., Mahar, J., Khan, M. J., Rasool, M. S., & Khan, M. Z. (2025). IN SILICO INVESTIGATION OF 3, 6-DIPHENYL-[1, 2, 4] TRIAZOLO [3, 4-B][1, 3, 4] THIADIAZOLE DERIVATIVES AS EGFR MODULATORS FOR LUNG CANCER TREATMENT. *The Cancer Research Review*, *4*(2), 243-308.
23. Abbas, M. A. (2025). Advanced Synthesis and Multifunctional Characterization of Neodymium-Doped $Ba_2NiCoFe_{28-x}O_{46}$ X-Type Hexagonal Ferrites: A Comprehensive Study of Structural, Morphological, and Electromagnetic Properties. *Sch Acad J Biosci*, *8*, 1213-1227
24. Huang, H., He, Y., Li, X., Li, M., Zeng, C., Dong, F., ... & Zhang, Y. (2015). Bi 2 O 2 (OH)(NO 3) as a desirable [Bi 2 O 2] 2+ layered photocatalyst: strong intrinsic polarity, rational band

https://scientia-nexus.org/index.php/jpcs
DOI: https://doi.org/10.5281/zenodo.19767807

An Open-Access Peer-Reviewed Journal

structure and {001} active facets co-beneficial for robust photooxidation capability. *Journal of Materials Chemistry A*, *3*(48), 24547-24556.

25. Iqbal, M. T., Saeeda, S., Zahra, T., Umar, Z., Khan, W. Z., Adnan, M., ... & Toffique, M. (2025). Next-generation materials discovery using DFT: functional innovation. *Sol. Energy Catal. Eco Toxic. Model. Sch J Eng Tech*, *7*, 454-486.
26. Ahmed, A., Fatima, A., Shakya, S., Rahman, Q. I., Ahmad, M., Javed, S., ... & Ahmad, A. (2022). Crystal structure, topology, DFT and Hirshfeld surface analysis of a novel charge transfer complex (L3) of anthraquinone and 4-{[(anthracen-9-yl) meth-yl] amino}-benzoic acid (L2) exhibiting photocatalytic properties: an experimental and theoretical approach. *Molecules*, *27*(5), 1724.
27. Li, K., He, Y., Chen, P., Wang, H., Sheng, J., Cui, W., ... & Dong, F. (2020). Theoretical design and experimental investigation on highly selective Pd particles decorated C3N4 for safe photocatalytic NO purification. *Journal of Hazardous Materials*, *392*, 122357.
28. Oliveira, M. C. D., Fonseca, V. S., Neto, N. A., Ribeiro, R. A. P., Longo, E., De Lazaro, S. R., ... & Bomio, M. R. D. (2020). Connecting theory with experiment to understand the photocatalytic activity of CuO–ZnO heterostructure. *Ceramics International*, *46*(7), 9446-9454.
29. Li, X., Maffettone, P. M., Che, Y., Liu, T., Chen, L., & Cooper, A. I. (2021). Combining machine learning and high-throughput experimentation to discover photocatalytically active organic molecules. *Chemical Science*, *12*(32), 10742-10754.
30. Mai, H., Le, T. C., Chen, D., Winkler, D. A., & Caruso, R. A. (2022). Machine learning for electrocatalyst and photocatalyst design and discovery. *Chemical Reviews*, *122*(16), 13478-13515.
31. Hussain, S., & Rehman, J. U. (2023). First-principles calculations to investigate structural, electronics, mechanical, and optical properties of KGaO3 cubic perovskite for photocatalytic water-splitting application. *Optik*, *291*, 171326.
32. Ni, Q., Ke, X., Qian, W., Yan, Z., Luan, J., & Liu, W. (2024). Insight into tetracycline photocatalytic degradation mechanism in a wide pH range on BiOI/BiOBr: Coupling DFT/QSAR simulations with experiments. *Applied Catalysis B: Environmental*, *340*, 123226.
33. Duan, X., Huang, Y., Shen, C., Jones, P., & Deng, X. (2025). Study on the sterilization performance of photocatalysts used in indoor air purification. *Indoor Air*, *2025*(1), 1071778.

https://scientia-nexus.org/index.php/jpcs
DOI: https://doi.org/10.5281/zenodo.19767807

An Open-Access Peer-Reviewed Journal

34. Xia, Y., Yang, H., Ho, W., Zhu, B., & Yu, J. (2024). Promoting the photocatalytic NO oxidation activity of hierarchical porous g-C3N4 by introduction of nitrogen vacancies and charge channels. *Applied Catalysis B: Environment and Energy*, *344*, 123604.

35. Pingak, R. K., Conquest, O. J., & Stampfl, C. (2025). A DFT investigation of photocatalytic water splitting properties of the InS/GaTe heterostructure: direct Z-scheme vs. traditional type-II. *Journal of Materials Chemistry A*, *13*(44), 38350-38368.

36. Zhang, X., Chen, A., Chen, L., & Zhou, Z. (2022). 2D materials bridging experiments and computations for electro/photocatalysis. *Advanced Energy Materials*, *12*(4), 2003841.

37. Alharshan, G. A., Aboraia, A. M., Uosif, M. A., Sharaf, I. M., Shaaban, E. R., Saad, M., ... & Elsenety, M. M. (2023). Optical band gap tuning, DFT understandings, and photocatalysis performance of ZnO nanoparticle-doped Fe compounds. *Materials*, *16*(7), 2676.

38. Thawarkar, S., Rondiya, S. R., Dzade, N. Y., Khupse, N., & Jadkar, S. (2021). Experimental and theoretical investigation of the structural and opto-electronic properties of Fe-doped lead-free Cs2AgBiCl6 double perovskite. *Chemistry–A European Journal*, *27*(26), 7408-7417.

39. Abbas, M. A., Mahar, J., Hameed, N., & Rasool, M. S. (2025). DFT-Guided Design of a Low-Band-Gap Pyrazoline Scaffold: The Critical Role of a Para-Nitro Substituent. *Multidisciplinary Surgical Research Annals*, *3*(3), 461-503.

40. Abbas, M. A., Mahar, J., Khan, M. J., Rasool, M. S., & Khan, M. Z. (2025). IN SILICO INVESTIGATION OF 3, 6-DIPHENYL-[1, 2, 4] TRIAZOLO [3, 4-B][1, 3, 4] THIADIAZOLE DERIVATIVES AS EGFR MODULATORS FOR LUNG CANCER TREATMENT. *The Cancer Research Review*, *4*(2), 243-308.

41. Abbas, M. A., Mahar, J., Rasool, M. S., Khan, M. J., & Khan, M. Z. (2025). The Dual Therapeutic Promise of Quinoa: Exploring Antidiabetic and Antioxidant Effects through Experimental and Computational Models. *Multidisciplinary Surgical Research Annals*, *3*(3), 504-544.

42. Abbas, M. A., Junaid, M. J. M., Rasool, M. S., & Mahar, J. (2025). Structural and NLO Properties of Novel Organic 4-Bromo-4-Nitrostilbene Crystal: Experimental and DFT Study. *International Research Journal of Management and Social Sciences*, *6*(4), 1-20.

43. Abbas, M. A., & Rasool, M. S. (2026). Eco-Friendly Synthesis of Ag–Co3O4 Nanoparticles for Visible-Light Photocatalysis and DFT-Based Nonlinear Optical Investigation. *Chemical Technology and Engineering Applications*, *1*(1), 23-34.

44. Junaid, M., Rasool, M. S., Abbas, M. A., & Mahar, J. (2024). Formulation Development and Evaluation of a Bilayered Tablet Containing Dapagliflozin and Metformin. *Global Research*

https://scientia-nexus.org/index.php/jpcs
DOI: https://doi.org/10.5281/zenodo.19767807

An Open-Access Peer-Reviewed Journal

Journal of Natural Science and Technology, *2*(3).

45. Akram, S., Abbas, M. A., Mahar, J., Rasool, M. S., & Junaid, M. INTERFACIAL DEFECT PASSIVATION AND PHOTOPHYSICAL ENGINEERING OF $CSPBCL_3$ QUANTUM DOTS VIA BISBENZIMIDAZOLIUM LIGANDS FOR ADVANCED ELECTRONIC DEVICES.
46. Abbas, M. A., Khan, M. Z., Atif, H. M., Shahzad, A., & Mahar, J. (2025). Computer-Aided Analysis of Oxino-bis-Pyrazolederivative as a Potential Breast Cancer Drug Based on DFT, Molecular Docking, and Pharmacokinetic Studies: Compared with the Standard Drug Tamoxifen. *Indus Journal of Bioscience Research*, *3*(6), 535-537.